

AFML-TR-68-174

AD 674592

**MOMENTUM DISTRIBUTION IN THE DEBRIS
CLOUD PRODUCED BY HYPERVELOCITY
PERFORATION OF THIN PLATES**

**Capt. John H. Cunningham
Air Force Institute of Technology**

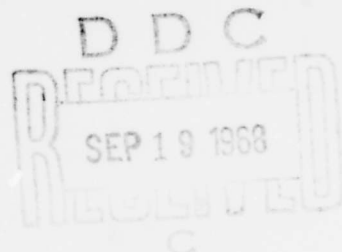
TECHNICAL REPORT AFML-TR-68-174

July 1968

This document has been approved for public release
and sale; its distribution is unlimited.

**Air Force Materials Laboratory
Air Force Systems Command
Wright-Patterson Air Force Base, Ohio**

Reproduced by the
CLEARINGHOUSE
for Federal Scientific & Technical
Information Springfield Va. 22151



NOTICES

When Government drawings, specifications, or other data are used for any purpose other than in connection with a definitely related Government procurement operation, the United States Government thereby incurs no responsibility nor any obligation whatsoever; and the fact that the Government may have formulated, furnished, or in any way supplied the said drawings, specifications, or other data, is not to be regarded by implication or otherwise as in any manner licensing the holder or any other person or corporation, or conveying any rights or permission to manufacture, use, or sell any patented invention that may in any way be related thereto.

ACQUISITION	
CFSTI	ACTION <input checked="" type="checkbox"/>
BDC	SECTION <input type="checkbox"/>
UNCLASSIFIED	<input type="checkbox"/>
JUSTIFICATION	
BY	
DISTRIBUTION AND AVAILABILITY CODES	
DIST.	SPECIAL
1	

Copies of this report should not be returned unless return is required by security considerations, contractual obligations, or notice on a specific document.

**MOMENTUM DISTRIBUTION IN THE DEBRIS
CLOUD PRODUCED BY HYPERVELOCITY
PERFORATION OF THIN PLATES**

**Capt. John H. Cunningham
Air Force Institute of Technology**

**This document has been approved for public release
and sale; its distribution is unlimited.**

BLANK PAGE


FOREWORD

This report was prepared by Capt. John H. Cunningham of the Air Force Institute of Technology as partial fulfillment of requirements for the degree Master of Science. The work was administered by Mr. Alan K. Hopkins of the Air Force Materials Laboratory under Project 7360, Chemistry and Physics of Materials, Task 736006, Hypervelocity Impact Studies.

The author gratefully acknowledges the assistance of members of the staff of the University of Dayton, particularly Mr. Hallock F. Swift for pertinent suggestions, timely advice and guidance, and the hypervelocity impact range staff headed by Mr. Lewis Shiverdecker, for their experimental assistance provided under Contract F33615-68-C-1138, Response of Materials to Pulse Loads. The author also wishes to thank his AFIT faculty advisors for their counsel and help in completing this report.

The manuscript was released by the author in July 1968 for publication as a Technical Report.

This technical report has been reviewed and is approved.


Herbert M. Rosenberg, Chief
Exploratory Studies Branch
Materials Physics Division
AF Materials Laboratory

ABSTRACT

An experimental investigation of the momentum distribution within the debris cloud produced by the impact of 3.17 mm spheres on 0.79 mm thick plates was conducted. Two independent experiments with projectile velocities ranging from 6.65 km/sec to 7.25 km/sec were completed in an attempt to determine momentum distribution. Small metal plates were impacted by the cloud for measurement of the incident momentum. A ballistic pendulum was used in an attempt to capture small segments of the debris cloud and to measure the momentum distribution in the cloud itself. The momentum intensity, as a function of distance from the center of the debris cloud, was determined in each experiment and the results were compared and evaluated.

Contents

	Page
Forward	ii
Abstract	iii
List of Figures	vi
List of Tables	ix
I. Introduction	1
Background	1
Purpose	6
II. Experimental Procedure	7
Approach to the Problem	7
Flyer Plate Test Series	7
Primary Flyer Plate Experiments	9
Results	13
Ballistic Pendulum Measurements	28
Results	38
III. Discussion of Results and Conclusions	46
IV. Recommendations	56
Bibliography	58
Appendix A: Description of Equipment	60
AFML Light Gas Gun	60
Streak Camera Winker System	62
Image Converter Camera System	62
Flash X-ray System	63
Appendix B: Flyer Plate Test Series	66
Results	66

Contents (Continued)

	Page
Appendix C: Ballistic Pendulum Calibration	76
Logarithmic Decrement	76
Deviation Analysis	80
Appendix D: Table Summary of Flyer Plate and Ballistic Pendulum Rounds	84

List of Figures

Figure		Page
1	Near Earth Meteoroid Environment	2
2	Sequential Photographs of Simulated Meteoroid Impact	3
3	Momentum Multiplication from Thin Plate Impact . . .	4
4	Assumed Momentum Intensity Distribution	8
5	Flyer Plate Experimental Configuration	10
6	Orientation of Flyer Plates	11
7	Photograph of Flyer Plates Prior to Impact.	11
8	Flyer Plate Experiment Circuitry	12
9	Sequential Radiograph of Impacted Flyer Plates, AFML Round No. 2383	14
10	Radiograph of Grid Used for Flyer Plate Measurement	15
11	Location of Debris Cloud Center.	16
12	Momentum Intensity vs Distance from Debris Cloud Center, AFML Round No. 2383	18
13	Total Momentum vs Distance from Debris Cloud Center, AFML Round No. 2383	18
14	Sequential Radiograph of Impacted Flyer Plates, AFML Round No. 2402	20
15	Momentum Intensity Distance to Debris Cloud Center, AFML Round No. 2402	22

List of Figures (Continued)

Figure	Page
16 Total Momentum vs Distance to Debris Cloud Center, AFML Round No. 2402	22
17 Sequential Radiograph of Impacted Flyer Plates, AFML Round No. 2406	24
18 Momentum Intensity vs Distance to Debris Cloud Center, AFML Round No. 2406	26
19 Total Momentum vs Distance to Debris Cloud Center, AFML Round No. 2406	26
20 Photograph of Impacted Flyer Plates	27
21 Ballistic Pendulum Construction	29
22 Ballistic Pendulum Cross Section	30
23 Ballistic Pendulum Suspension Detail	32
24 Photograph of Pendulum Calibration Setup	32
25 Ballistic Pendulum Experimental Configuration	33
26 Drawing of Splitter Plate	34
27 Photograph of Splitter Plate After Impact; Movable Plabe Attached	35
28 Detail of Mirror	36
29 Photographis Results of Ballistic Pendulum Experiments	40
30 Photograph of Impacted Polyethylene Plate	42
31 Photograph of Ballistic Pendulum	44
32 Momentum Intensity vs Distance to Debris Cloud Center: Ballistic Pendulum Results	45

List of Figures (Continued)

Figure	Page
33 Flyer Plate Data Compared with Results of Crater Volume - Energy Calculation	48
34 Comparison of Flyer and Pendulum Data: Copper Impact.	50
35 Comparison of Flyer and Pendulum Data: Aluminum Impact	50
36 Comparison of Flyer and Pendulum Data: Cadmium Impact.	51
37 Sequential Photographs of Cloud-Splitter Interaction	53
38 AFML Light Gas Gun.	61
39 Light Gas Gun Firing Sequence	61
40 Streak Camera Winker System.	64
41 Foil Contact Switch.	64
42 Rigid Flyer-Plate Holder	67
43 Impact Effect on Backup Plate.	67
44 Photographs of Impacted Flyer Plates	71
45 Pendulum Calibration Configuration	77
46 Calibration Circuit Diagram	79
47 Photographs for Decrement Calculations	79
48 Geometry of Deviation Analysis	81

List of Tables

Tables		Page
I	Shock Heating Properties	2
II	Data from Round #2383, Impact of 3.17 mm Copper Projectile $V_p = 6.652 \text{ km/sec}$	17
III	Data from Round #2402, Impact of 3.17 mm Aluminum Sphere $V_p = 7.254 \text{ km/sec}$	21
IV	Data from Round #2406, Impact of 3.17 mm Cadmium Sphere $V_p = 7.054 \text{ km/sec}$	25
V	Ballistic Pendulum Results	41
VI	Weight Loss Data AFML Round No. 2352	72
VII	Flyer Data AFML Round No. 2357	72
VIII	Flyer Data AFML Round No. 2365	73
IX	Flyer Data AFML Round No. 2375	74
X	Flyer Data AFML Round No. 2380	75
XI	Pendulum Calibration Data	78
XII	Results of Deviation Analysis	83
XIII	Summary of Flyer Plate and Ballistic Pendulum Rounds	85

BLANK PAGE

MOMENTUM DISTRIBUTION IN THE DEBRIS
CLOUD PRODUCED BY HYPERVELOCITY
PERFORATION OF THIN PLATES

I. Introduction

To date, manned space missions have been limited to near earth orbits. Plans are being made for mans first landing on the moon. Missions away from the near earth environment mean an extended exposure of the spacecraft and its passengers to the hazards of meteoroid impact. Much work has been done to determine the exact nature of the meteoroid environment and a best estimate is shown in Fig. 1.

Once the environment is known the problem becomes one of designing an adequate means of vehicle protection. One of the more promising and more extensively investigated protection arrays is the Whipple Bumper Concept (Ref 7 :264). A simulated impact of a meteoroid on a Whipple bumper is shown in Fig. 2.

The meteoroid approaches the bumper from the right. Upon impact, the projectile and the bumper are shocked and heated. Depending upon the properties of the projectile and bumper, the resultant debris cloud will be composed of different percentages of particulate, liquid and gaseous debris. Table I demonstrates the different effects of pressure on materials with different physical properties. Cadmium for example will vaporize at lower impact

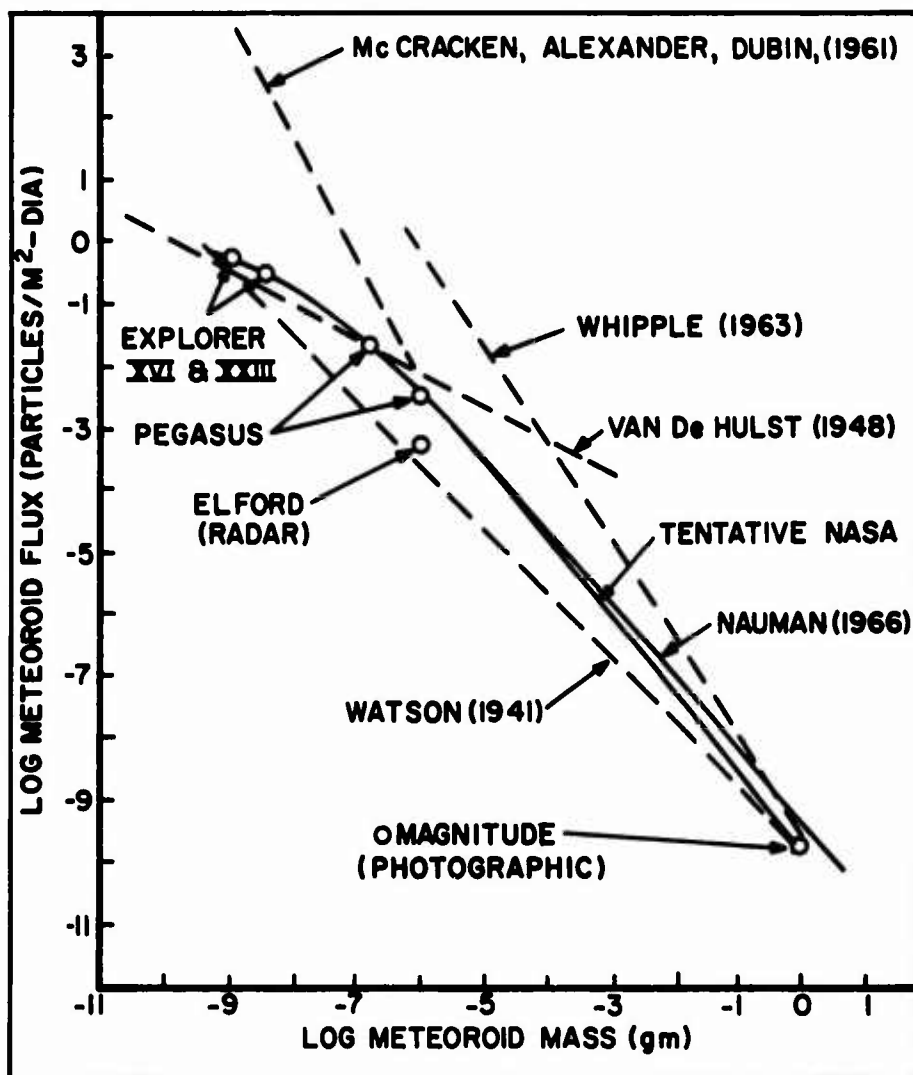


Fig. 1. Near Earth Meteoroid Environment
(Ref 7: 243)

Material	Melting Temp ^{°C}	Vaporization Temp ^{°C}	Pressure to cause incipient melting (M bar)	Pressure to cause complete melting (M bar)	Pressure to cause vaporiz- ation (M bar)
Aluminum	660	2057	0.6	0.9	-----
Cadmium	321	767	0.4	0.46	0.8
Copper	1083	2336	1.4	1.8	-----

Shock Heating Properties

Table I

(Ref 9:231)

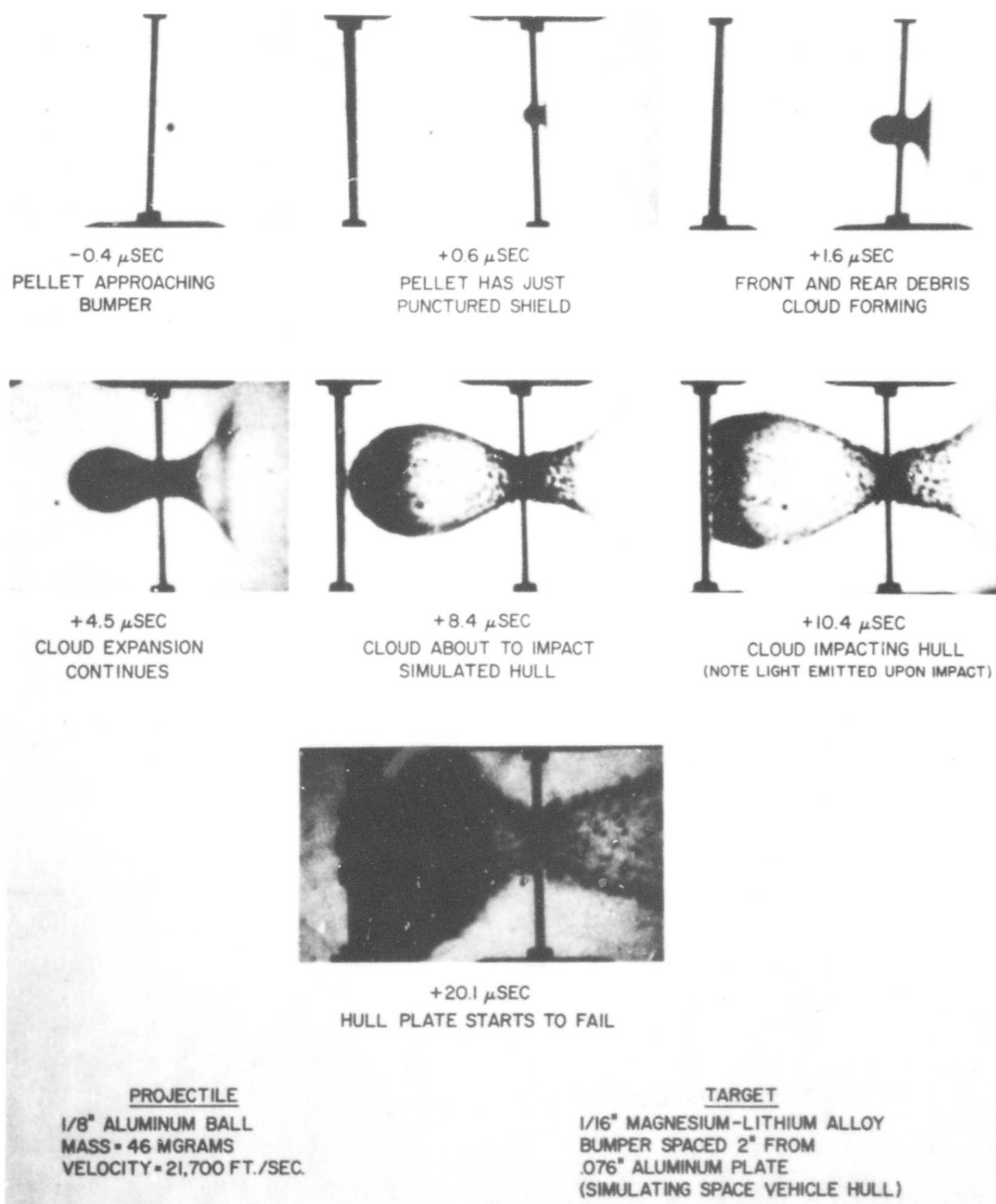


Fig. 2. Sequential Photographs of
Simulated Meteoroid Impact

pressures than either aluminum or copper. The purpose of the bumper is to disintegrate the meteoroid and spread its energy and momentum over a large area of the hull plate.

The momentum of the debris cloud is some multiple of the momentum of the meteoroid because, as the projectile impacts the bumper, debris is thrown upstream as well as downstream (see Fig. 3). From conservation of momentum

$$M_p V_p = P_{dc} - P_u \quad (1-1)$$

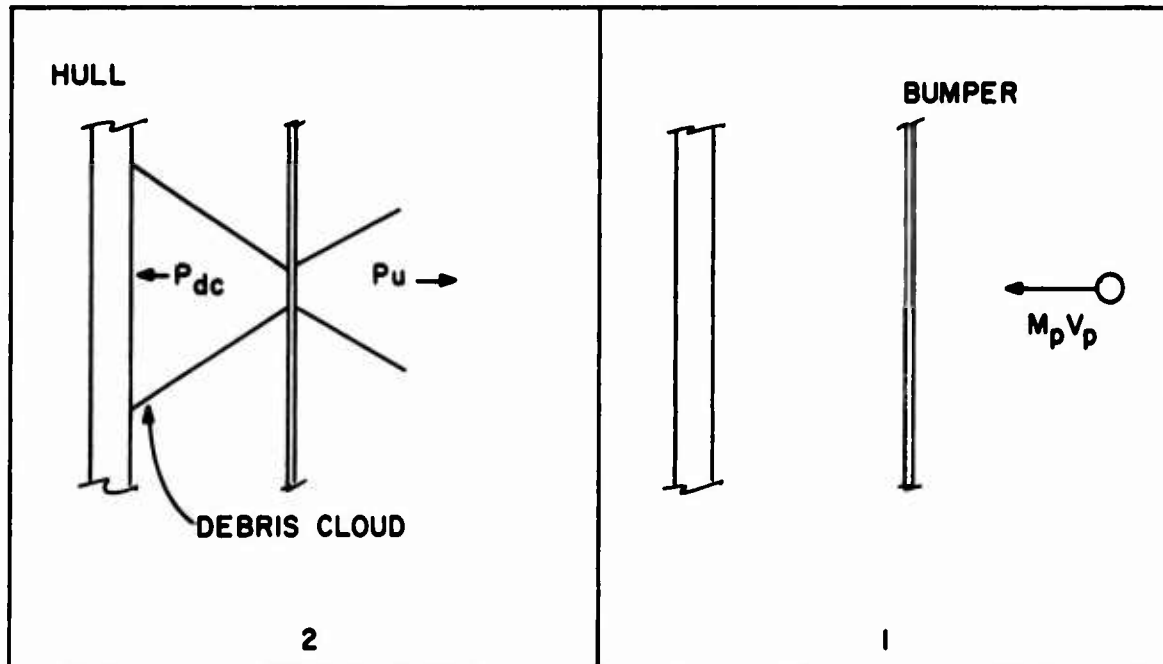


Fig. 3. Momentum Multiplication
From Thin Plate Impact

where P_{dc} is the momentum of the debris cloud,

P_u = momentum of upstream cloud,

and $M_p V_p$ = momentum of projectile.

$$\text{Thus } P_{dc} = M_p V_p + P_u \quad (1-2)$$

$$\text{and } P_{dc} = M_p V_p \left(1 + \frac{P_u}{M_p V_p}\right). \quad (1-3)$$

As the debris cloud impacts the hull plate, cratering occurs and debris rebounds causing a second momentum multiplication.

The damage from the impact of the debris cloud can be similar to the damage caused by regular meteoroid impacts. The hull plate can fail by penetration, spalling, or buckling (Ref 3:101). The hull plate must then be designed with sufficient strength to withstand the increased momentum of the debris cloud and to prevent failure in one of the three modes.

Present projectile launching techniques are limited to approximately 10 km/sec projectile velocity. Meteoroids in space have velocities relative to the Earth of from 11 km/sec to 72 km/sec (Ref 7:244). One problem of the experimenter is to attempt to simulate effects of the meteoroid impacts at much higher velocities than can be attained in the laboratory. The answer at present lies in the correlation of low velocity experimental data with hydrodynamic models using Particle in Cell codes (Ref 1.). If this correlation is accomplished, a partially verified theory will be available to permit extra-

pulation to higher velocities. A reasonable system of meteoroid protection can then be designed for extended space voyages.

Purpose

It was the purpose of this investigation to experimentally determine the momentum distribution properties of debris clouds caused by the hypervelocity impact of spheres on thin metal plates. The information obtained is to be compared with theoretical solutions of the shield impact problem for confirmation and an improved understanding of the properties of debris clouds.

Investigated were the impacts of 3.17 mm spheres on 0.79 mm thick plates of like materials. Cadmium, Copper, and Aluminum were the materials used.

II. Experimental Procedure

Approach to the Problem

The attempt to determine debris cloud momentum was divided into two phases. The first phase involved the use of small metal flyer-plates for measuring the momentum experienced by individual regions of the simulated vehicle hull. This measurement includes two multiplication effects. A second experiment was designed which could eliminate the second multiplication effect by capturing small segments of debris clouds within a ballistic pendulum. The flyer plate experiments were conducted first because of their relative simplicity and the need to obtain a preliminary indication of the actual momentum distribution for use in the ballistic pendulum design.

Flyer Plate Test Series

A test series of five rounds was conducted to determine the experimental configuration best suited for the flyer-plate experiment. Preliminary calculations were completed in an attempt to determine the expected velocities of the flyer plates. A total multiplication factor of 1.5 and a linear momentum distribution (Fig. 4) on a plane parallel to the bumper were assumed for a copper debris cloud. The expected dimensions of the debris cloud were estimated from work done by Carey (Ref 3:37). The size and material of the flyer-plates was determined from stability and handling requirements.

Aluminum flyer plates (.635 cm x .635 cm x .318 cm) weighing approximately 350 mg were used in all flyer-plate shots. Copper was chosen as the material for use in the initial test series because of its high mass density (8.96 gm/cm^3) and low toxicity in comparison with cadmium.

Two configurations of plate holders were tried. The use of a rigid plate to support the flyer plates prior to impact proved unsatisfactory (see Appendix B). The use of a thin (.0025 cm thick) aluminum strip to support the flyer plates proved satisfactory and was the method used on all succeeding rounds. The preliminary calculation of

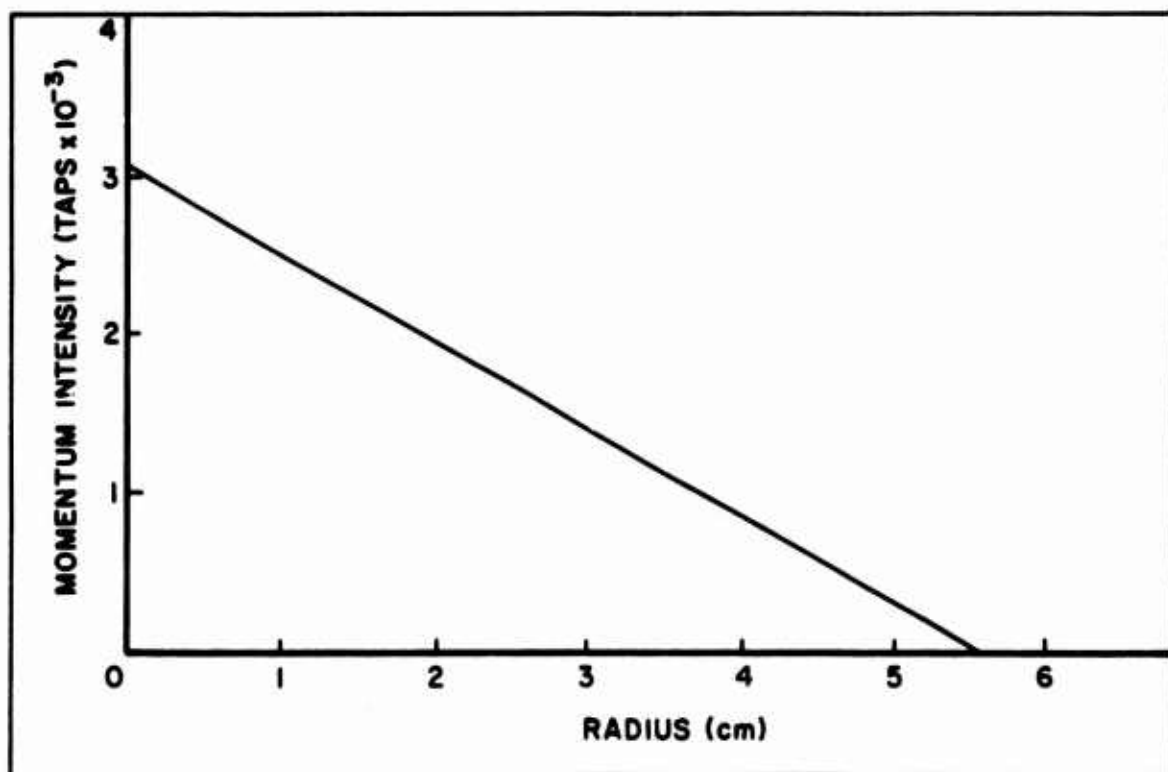


Fig. 4. Assumed Momentum Intensity Distribution

expected cloud momentum density proved to be a good approximation. Problems encountered with the x-rays occupied the remaining five test rounds.

Primary Flyer-Plate Experiments

Upon the completion of the test series, three primary rounds were completed using the final experiment configuration shown schematically in Fig. 5. The fourteen flyer plates were located 10.16 cm from the bumper (Fig. 6) and were arranged along the foil strip as shown in Fig. 7. The orientation of the flyer plates was designed to avoid debris impacting on the sides of the flyer plates.

The flight of the impacted flyer plates was monitored with sequential 105 kv flash x-rays* with exposure times short enough to prevent motion blurring of the plate images. The x-ray tube heads were located above the flyer plates and aimed toward the x-ray film located beneath the flyer-plate trajectories. The x-rays were controlled through the circuitry shown in Fig. 8. A contact switch was mounted on trajectory in front of the bumper plate. The contact switch (as described in Appendix A) was constructed of thin sheets of material that would provide a minimum disruption of the projectile. The x-ray times in relation to impact were monitored with an oscilloscope and the streak camera winker system (described in Appendix A).

* Field Emission Corporation Model 231.

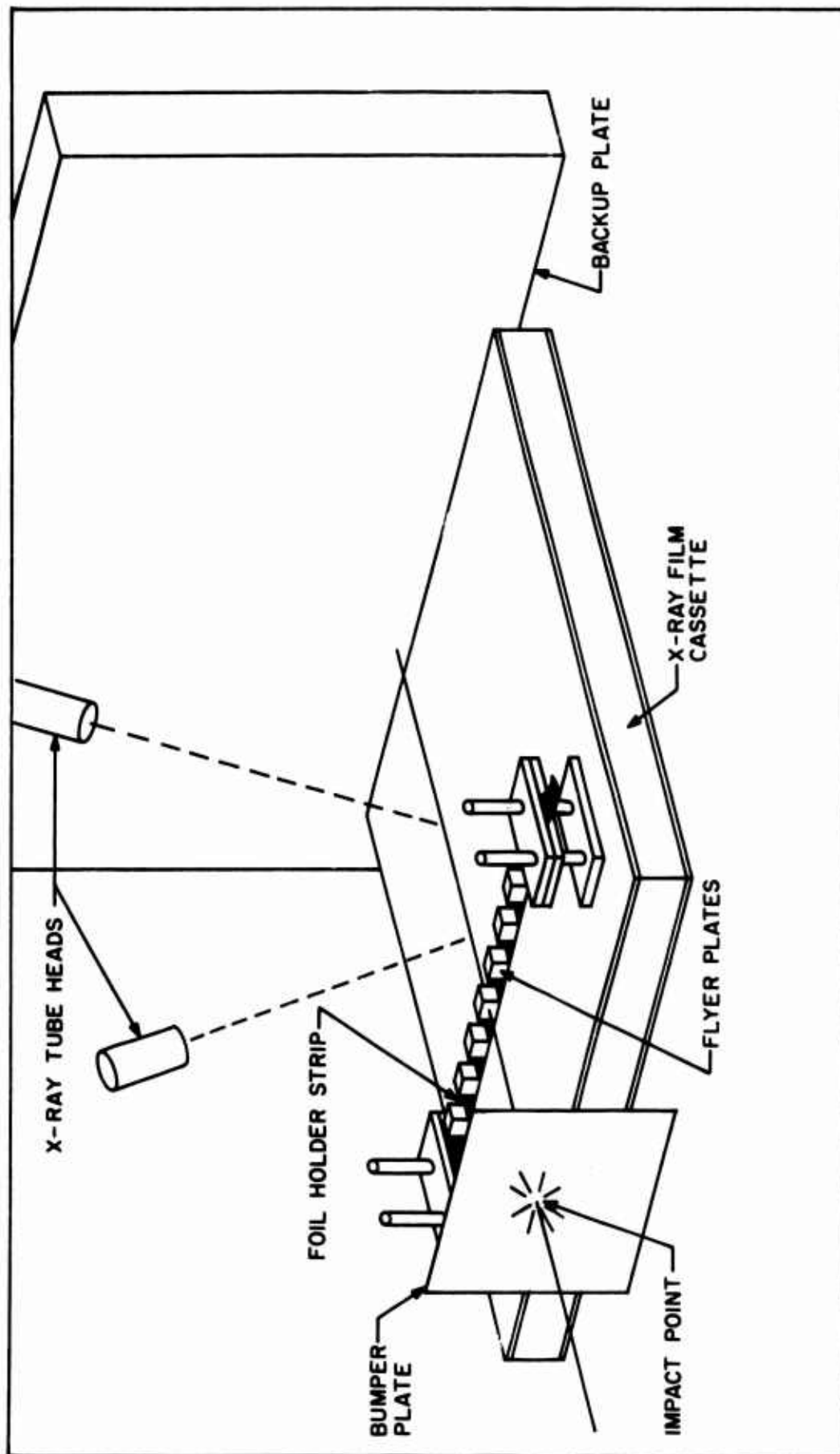


Fig. 5. Flyer Plate Experimental Configuration

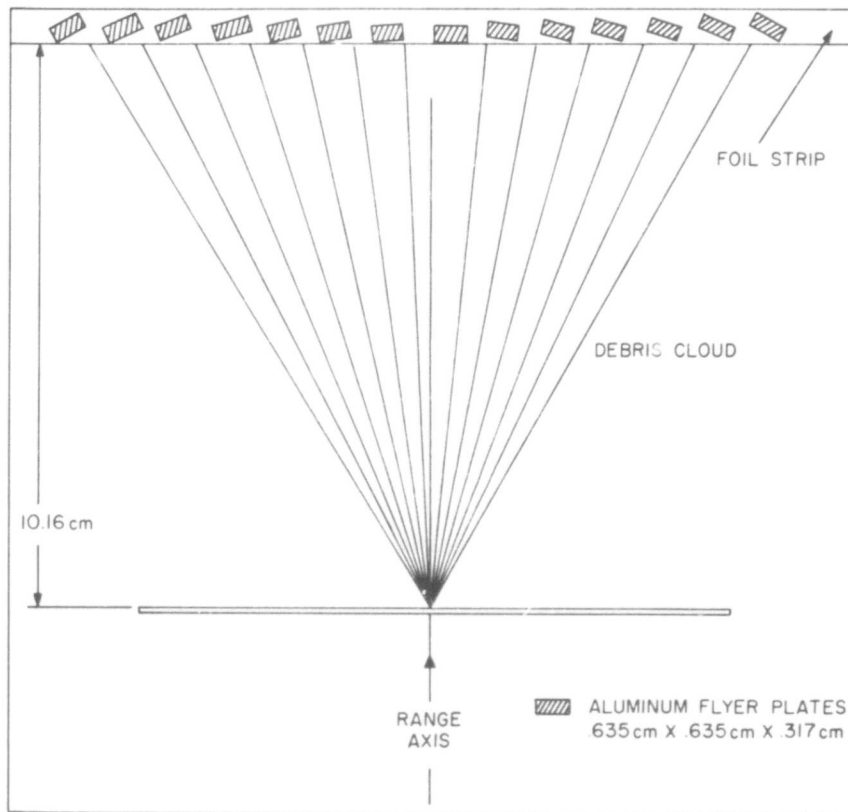


Fig. 6. Orientation of Flyer Plates

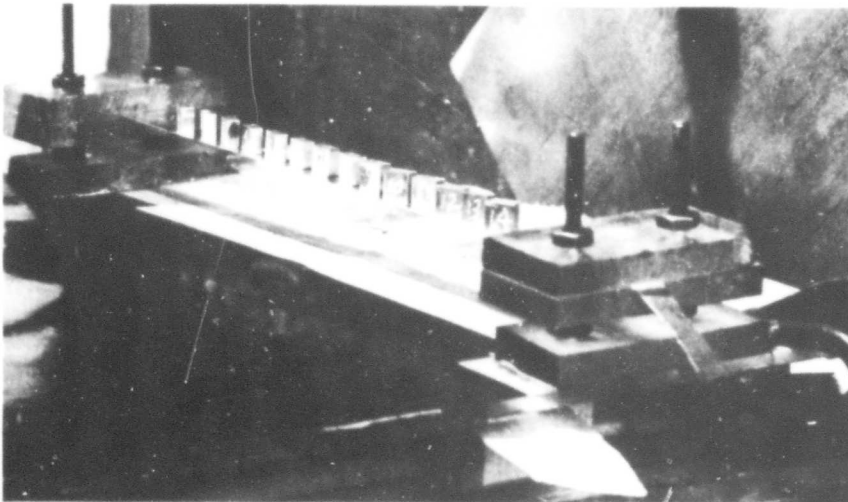


Fig. 7. Photographs of Flyer Plates Prior to Impact

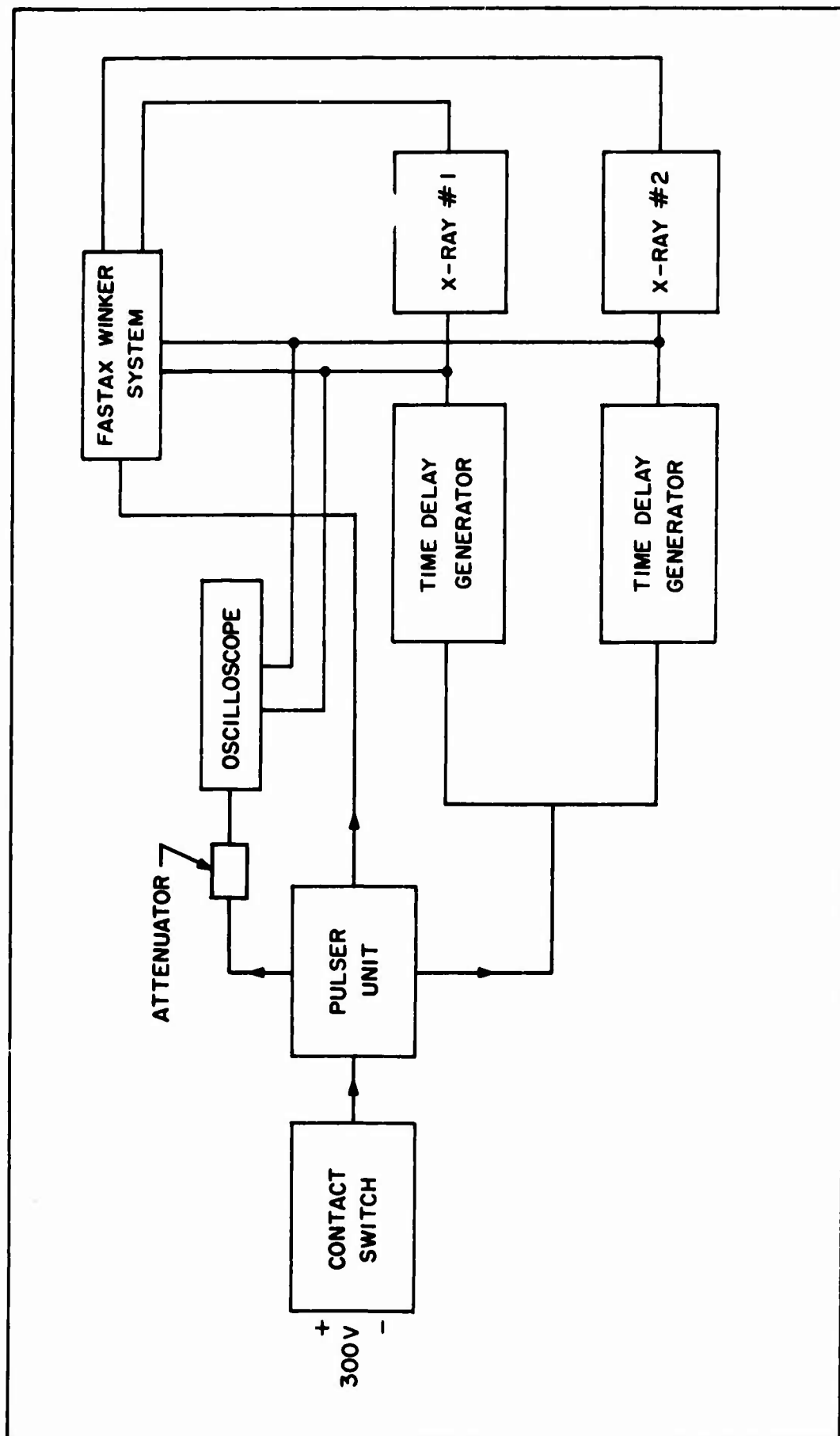


Fig. 8. Flyer Plate Experiment Circuitry

Results

The results of the three primary flyer-plate rounds will be discussed in the original firing sequence.

Round No. 2383. A copper sphere ($V_p = 6.652$ km/sec) impacted a copper bumper. The x-ray results are shown in Fig. 9. The time between x-rays was 1.5×10^{-3} sec. The change in flyer-plate position was determined by comparing the x-ray results with preliminary x-rays of a grid placed in the plane of flyer-plate trajectories (see Fig. 10). A base line was chosen from the grid and the change in position was calculated. The momentum of each plate (P_F) was then determined from change in position (L), time between exposures (T), and mass of the plate (M_2).

$$P_F = \frac{M_2 L}{T} \quad (2-1)$$

The momentum intensity (MI) was determined by dividing the plate momentum by its cross sectional area (A):

$$MI = \frac{P_F}{A} = \frac{P_F \text{ gm cm/sec}}{A \text{ cm}^2} \quad (2-2)$$

$$\text{Note: } 1 \text{ tap} = \frac{1 \text{ gm cm}}{\text{sec cm}^2} = \frac{1 \text{ dyne sec}}{\text{cm}^2}$$

The projectile impact was slightly off optimum trajectory which caused a requirement for locating the center of the momentum distribution. The point of impact was projected to the plane of the flyer plates as shown in Fig. 11. The distance of each plate from the center of the debris cloud was then measured directly from the scale drawing. The momentum intensity was thus determined as a function of

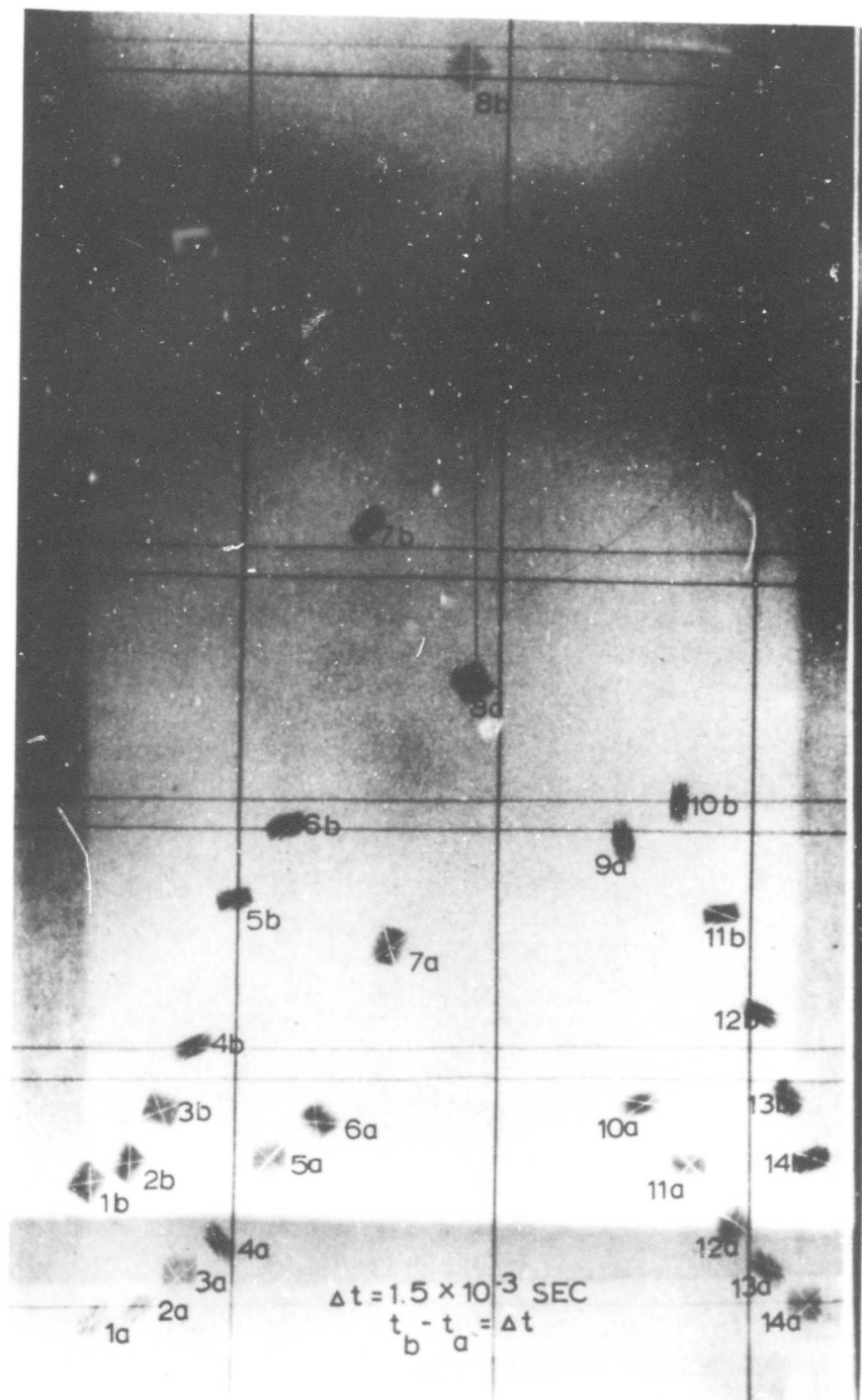


Fig. 9. Sequential Radiograph of Impacted Flyer Plates, AFML Round No. 2383

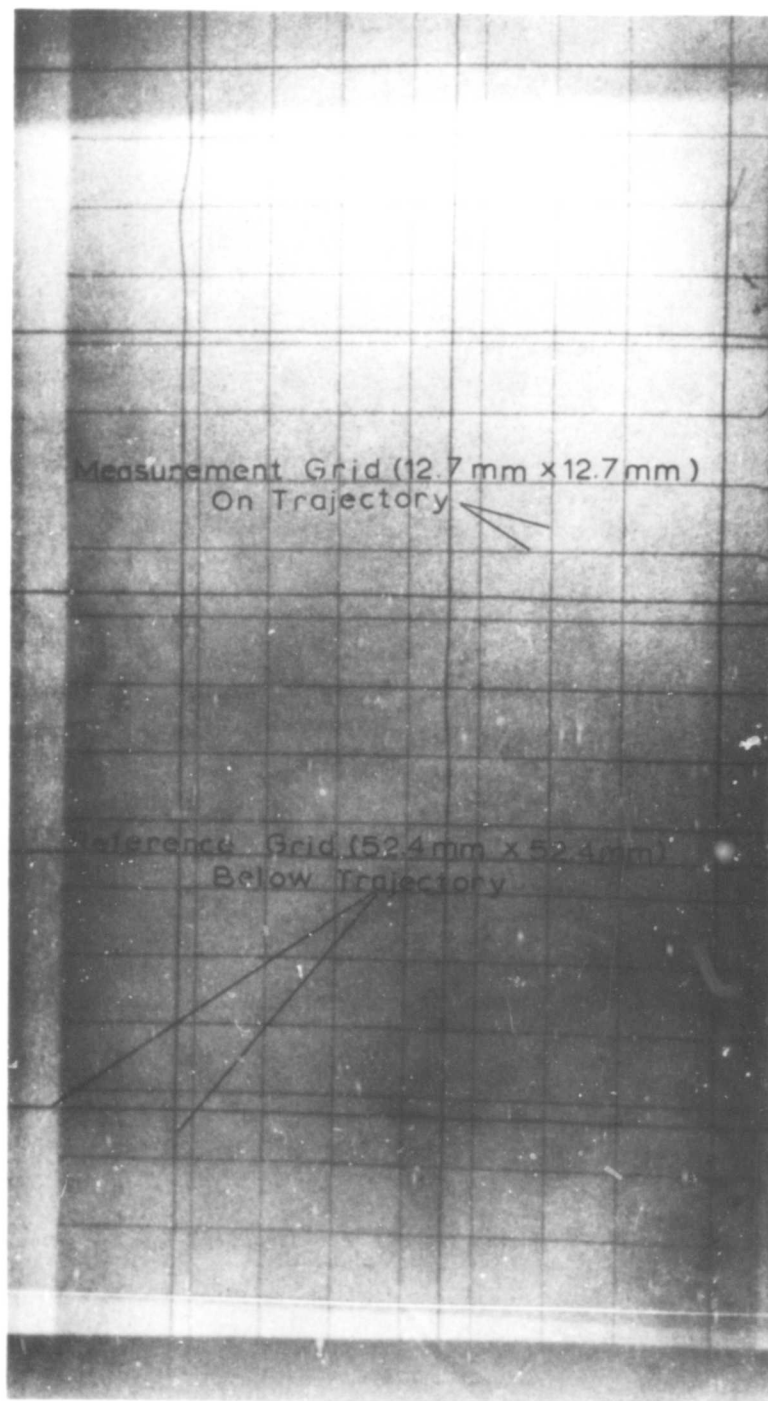


Fig. 10. Radiograph of Grid Used
For Flyer Plate Measurement

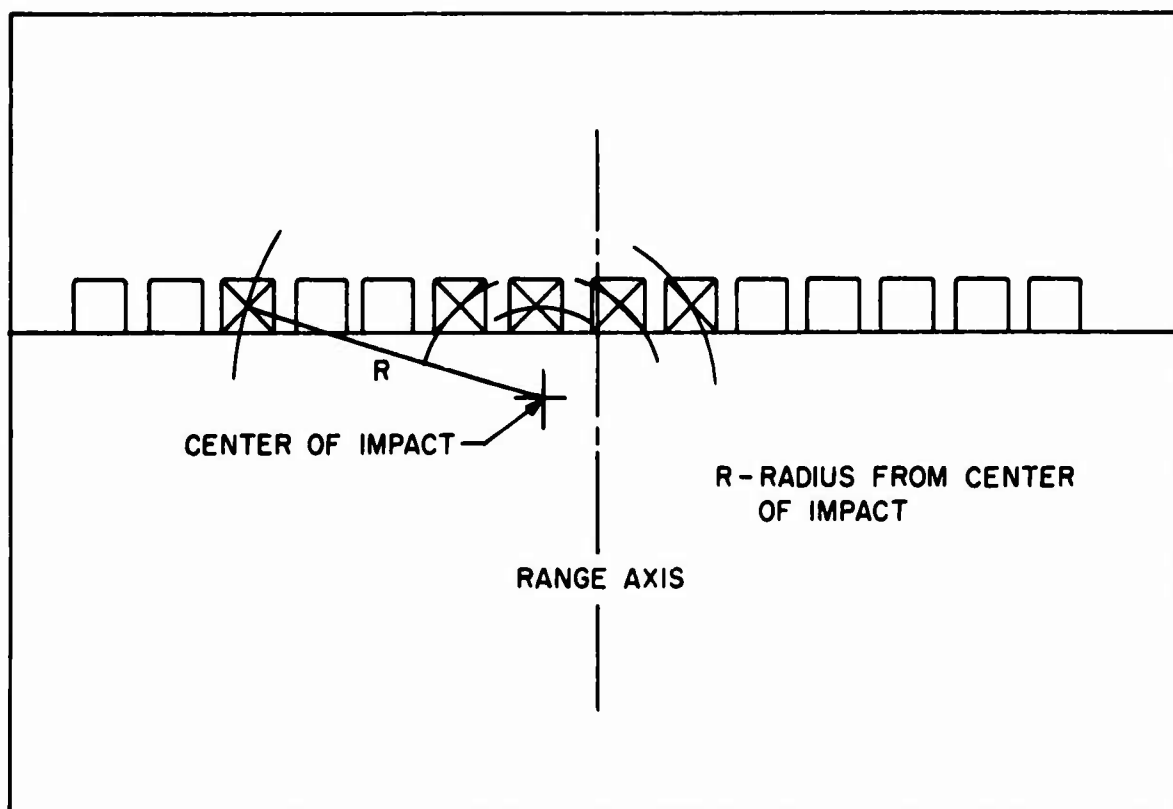


Fig. 11. Location of Debris Cloud Center

distance (R) from the center of the debris cloud.

The results for Round No. 2383 are shown in Table II and in Fig. 12. The flyer plates from Round 2383 were examined after the experiment and were observed to have suffered weight losses which were increasingly large as the plate location approached the center. No spalling was expected or discovered on any of the plates.

Each plate was retrieved after impact and reweighed. The second weights were then used in the momentum calculations. The use of the post-impact mass is justified because of the nature of the debris cloud impact. The duration of the impulse on the flyer plates is less than 1 micro-sec. This was determined by dividing the thickness

Plate Number	Distance to Center of Impact (cm)	Initial Mass (mg)	Final Mass (mg)	Velocity (m/sec)	Momentum Intensity (Taps)
1	5.32	355.4	355.0	3.74	329
2	4.37	356.3	355.6	6.71	592
3	3.42	341.9	340.5	11.75	992
4	2.47	362.3	359.2	17.01	1515
5	1.52	355.1	350.6	23.28	2024
6	.67	352.0	339.0	49.57	4166
7	.28	354.9	338.4	63.10	5295
8	1.39	357.0	347.5	38.77	3341
9	2.34	332.7	329.0	22.18	1810
10	3.29	339.6	336.8	17.75	1483
11	4.24	356.0	354.7	9.49	836
12	5.19	340.7	340.0	6.23	526
13	6.14	351.0	350.3	4.11	357
14	7.09	355.9	355.3	2.49	219

Data From Round #2383

Impact of 3.17 mm Copper Projectile $V_p = 6.652$ km/sec

Table II

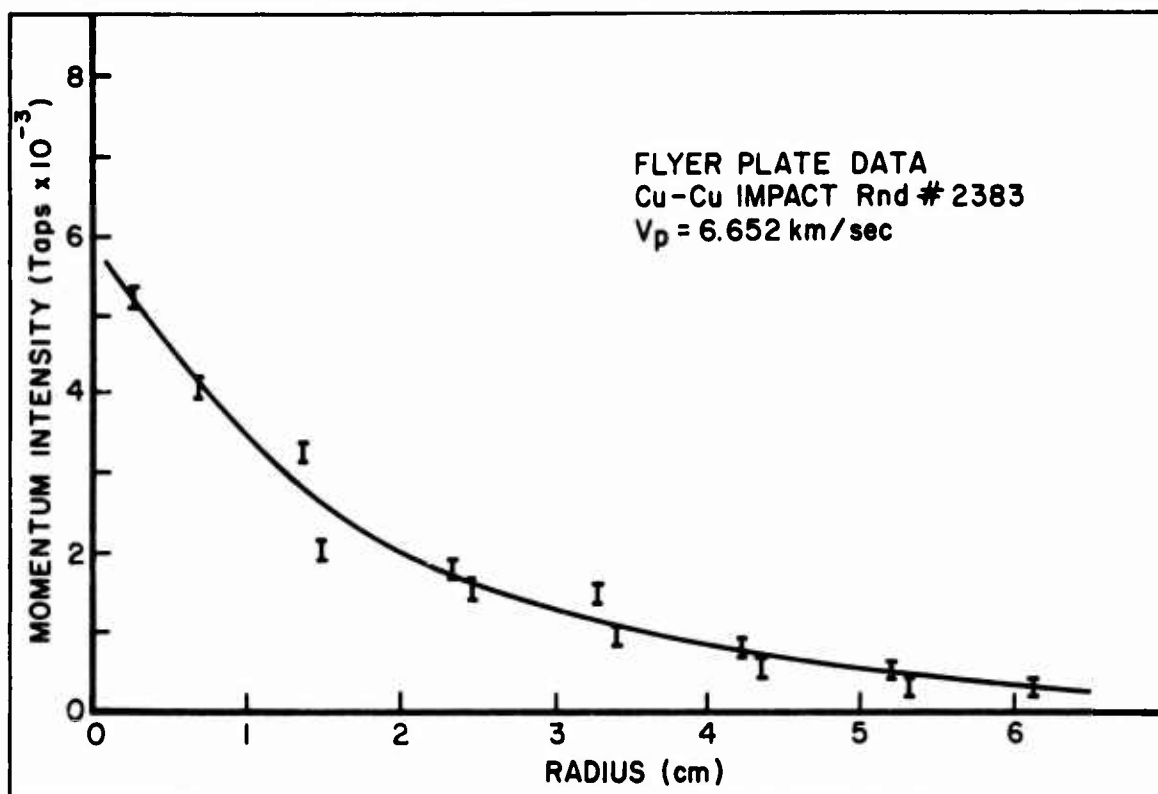


Fig. 12. Momentum Intensity vs Distance From Debris Cloud Center, AFML Round No. 2383

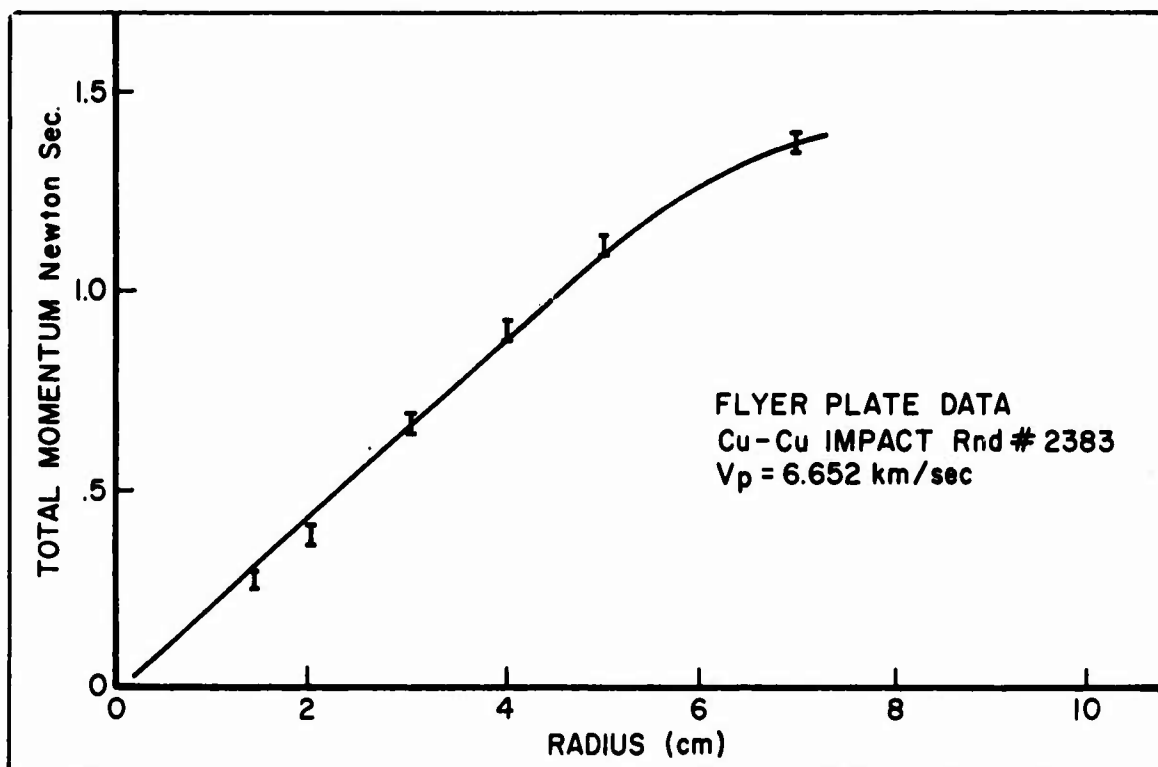


Fig. 13. Total Momentum vs Distance From Debris Cloud Center, AFML Round No. 2383

of a cloud segment by its velocity (see Fig. 37). The acceleration of the plates to their final velocity is almost instantaneous. The mass loss inflicted on the plate is, however, completed prior to any significant movement of the flyer plates. Simple calculations of the force due to the impulse of the cloud using Newton's Second Law, indicate that the most severely impacted flyer plate travels 3.15×10^{-3} cm during impact.

The momentum intensity was concentrated in the center and gradually decreased toward the edges. The total momentum of the cloud was calculated by integrating the momentum intensity curve (Fig. 12) through 360° using the trapezoid rule (Ref 11: 551). The cumulative momentum as a function of cloud radius is shown in Fig. 13. The curve approximates a straight line but levels off as the extreme edge of the measured debris cloud is approached. Total momentum calculations included only the measured section of the cloud. No attempt was made to extend the total momentum calculations to points outside the extreme flyer plates. The multiplication factor M.F. was calculated by dividing the total momentum (P) by the input momentum ($M_p V_p$)

$$M.F. = \frac{P}{M_p V_p} \quad (2-3)$$

For Round 2383 (M.F. equaled 1.372).

Round No. 2402. The analysis of Round No. 2402

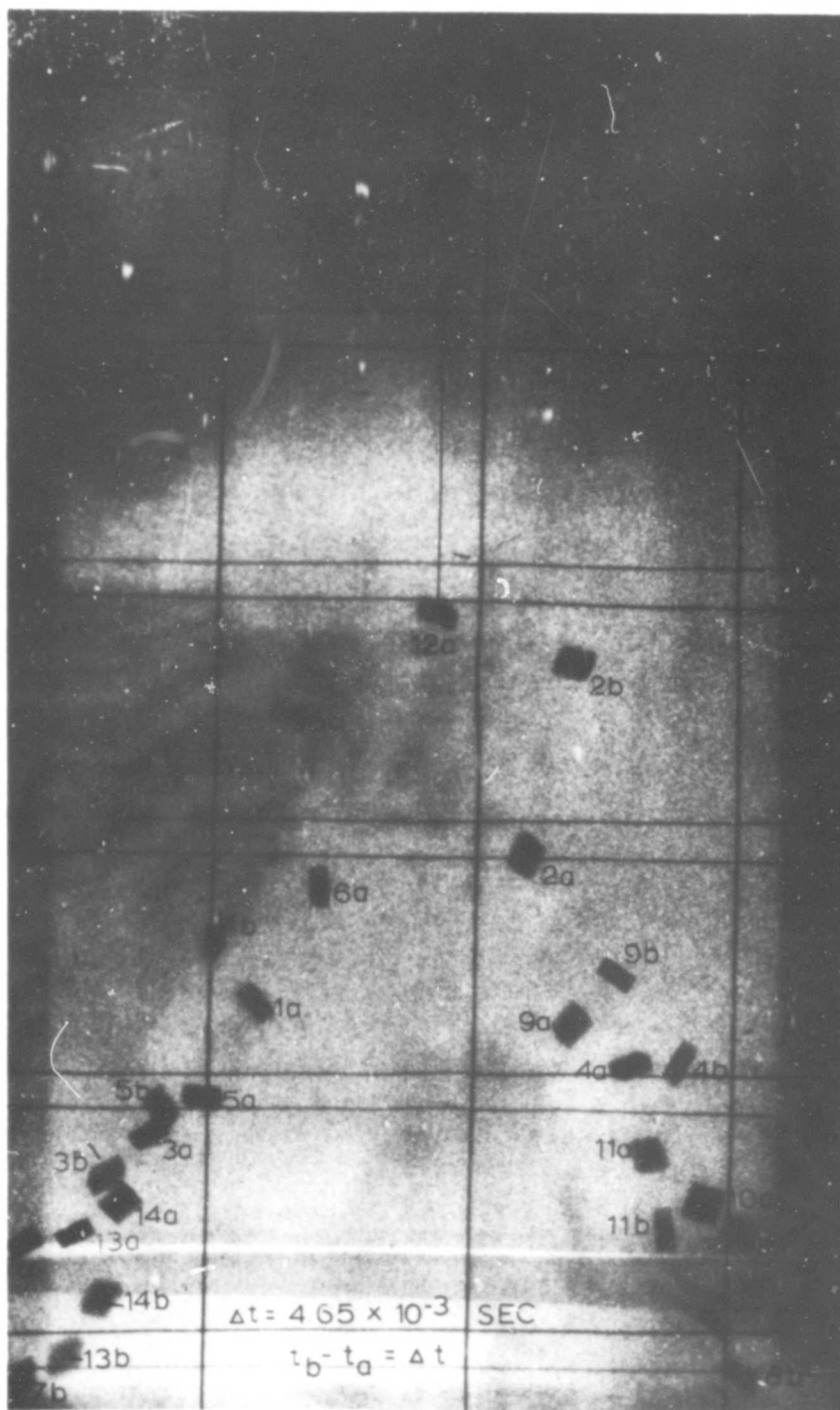


Fig. 14. Sequential Radiograph of Impacted Flyer Plates, AFML Round No. 2402

Plate Number	Distance to Center of Impact (cm)	Initial Mass (mg)	Final Mass (mg)	Velocity (m/sec)	Momentum Intensity (Taps)
13	4.58	329.3	329.1	.342	27.9
14	3.68	332.5	332.1	2.15	177.1
3	2.73	343.5	343.4	5.18	441
5	1.80	350.0	349.3	6.97	604
1	.86	358.3	356.5	12.83	1134
6	.15	360.0	355.3	22.81	2010
12	1.17	362.0	359.6	11.99	1069
2	2.13	354.4	353.4	7.93	695
9	3.04	353.0	352.4	4.48	391
4	4.02	337.0	337.0	3.33	278
11	4.95	334.9	334.8	1.42	118
10	5.88	329.5	329.6	.290	23.7

Data From Round #2402

Impact of 3.17 mm Aluminum Sphere $V_p = 7.254$ km/sec

Table III

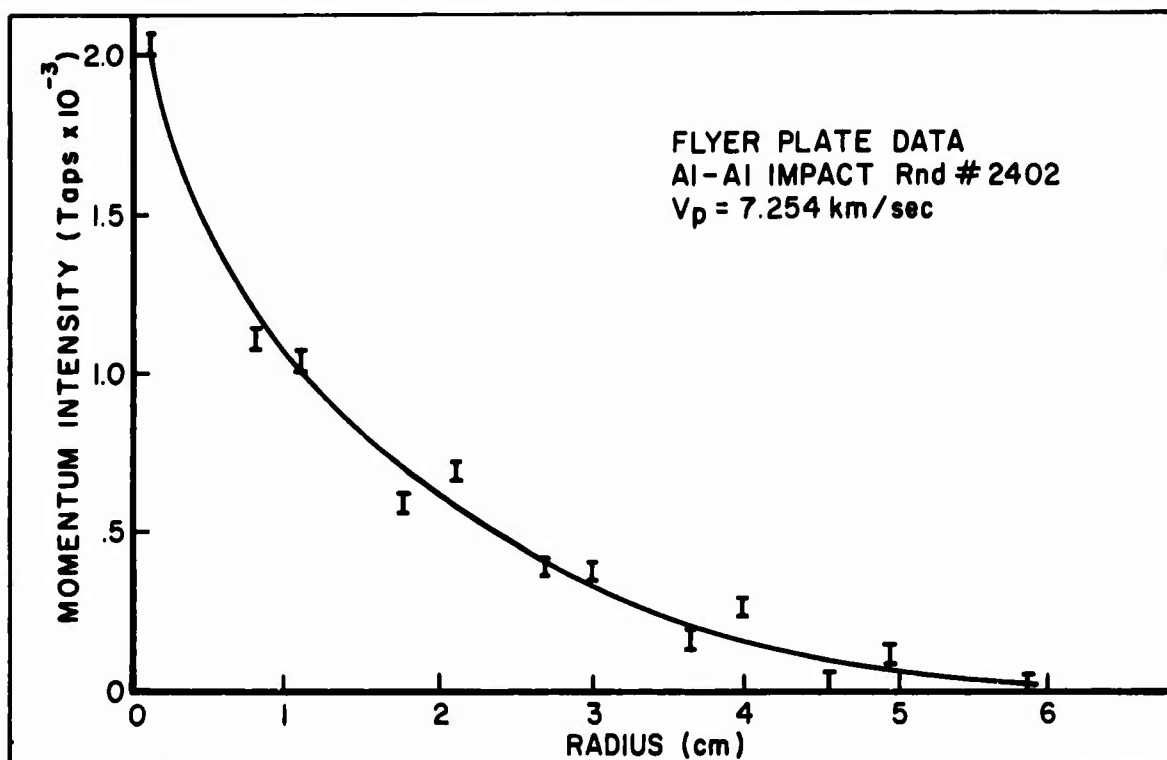


Fig. 15. Momentum Intensity vs Distance to Debris Cloud Center, AFML Round No. 2402

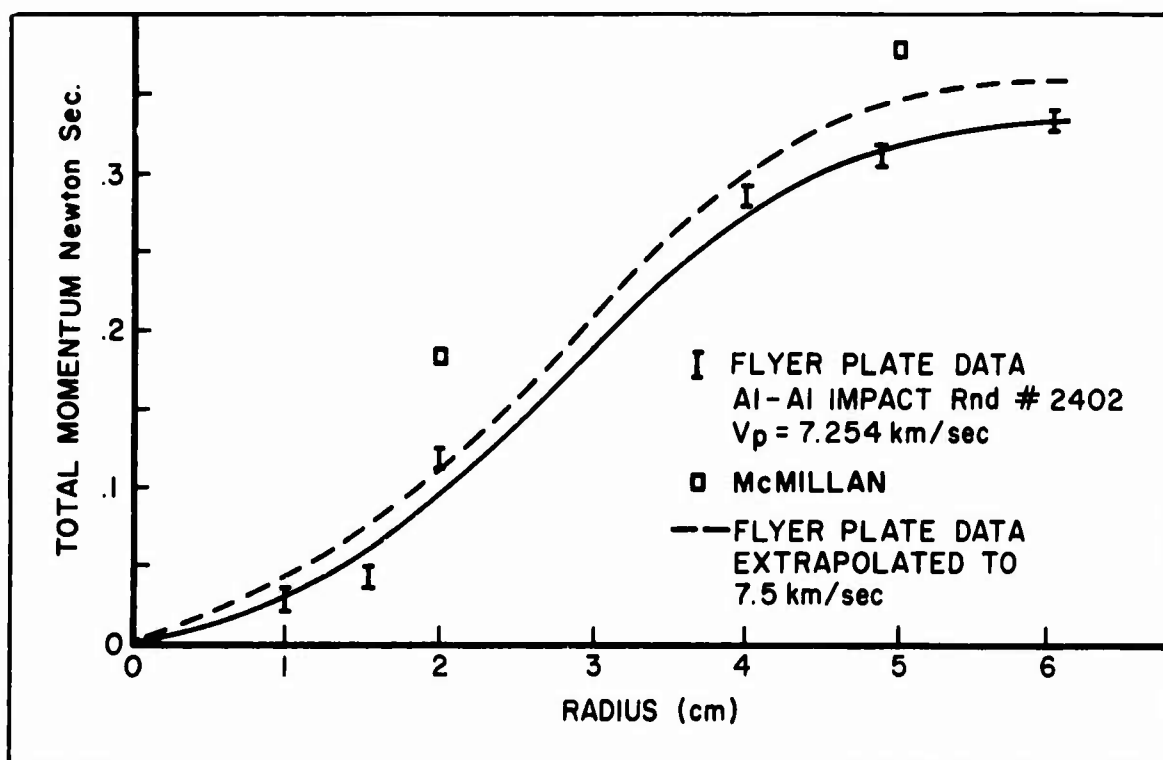


Fig. 16. Total Momentum vs Distance to Debris Cloud Center, AFML Round No. 2402

(Aluminum-Aluminum Impact, $V_p = 7.254$ km/sec) was conducted in the same manner as that of Round No. 2383. The x-ray results are shown in Fig. 14 and the momentum intensity data are presented in Table III. The momentum intensity distribution is shown in Fig. 15 and total momentum plotted in Fig. 16. As in Round No. 2383 the total momentum curve levels at the edge of the measured cloud. The aluminum did not display cloud symmetry to the same degree as did the copper. M.F. for the aluminum was 1.099 which as expected was less than that for copper. Because of the low momentum intensity of the aluminum debris cloud less mass loss was experienced by the flyer plates in Round No. 2402. Consequently a smaller multiplication effect was experienced by the plates impacted by the Aluminum cloud.

Round No. 2406. The last flyer plate round was a cadmium-cadmium impact with $V_p = 7.045$ km/sec. The results from the x-rays and momentum intensity calculations are presented in Fig. 17 and Table IV. The momentum intensity and total momentum distributions are plotted in Figs. 18 and 19. The multiplication factor for the cadmium was 1.635. This value does not include any estimate of the momentum contained outside the radius of measurement.

The flyer plates were retrieved and reweighed as in the other rounds. The flyer plates impacted by the cadmium cloud showed signs of very fine cratering plus

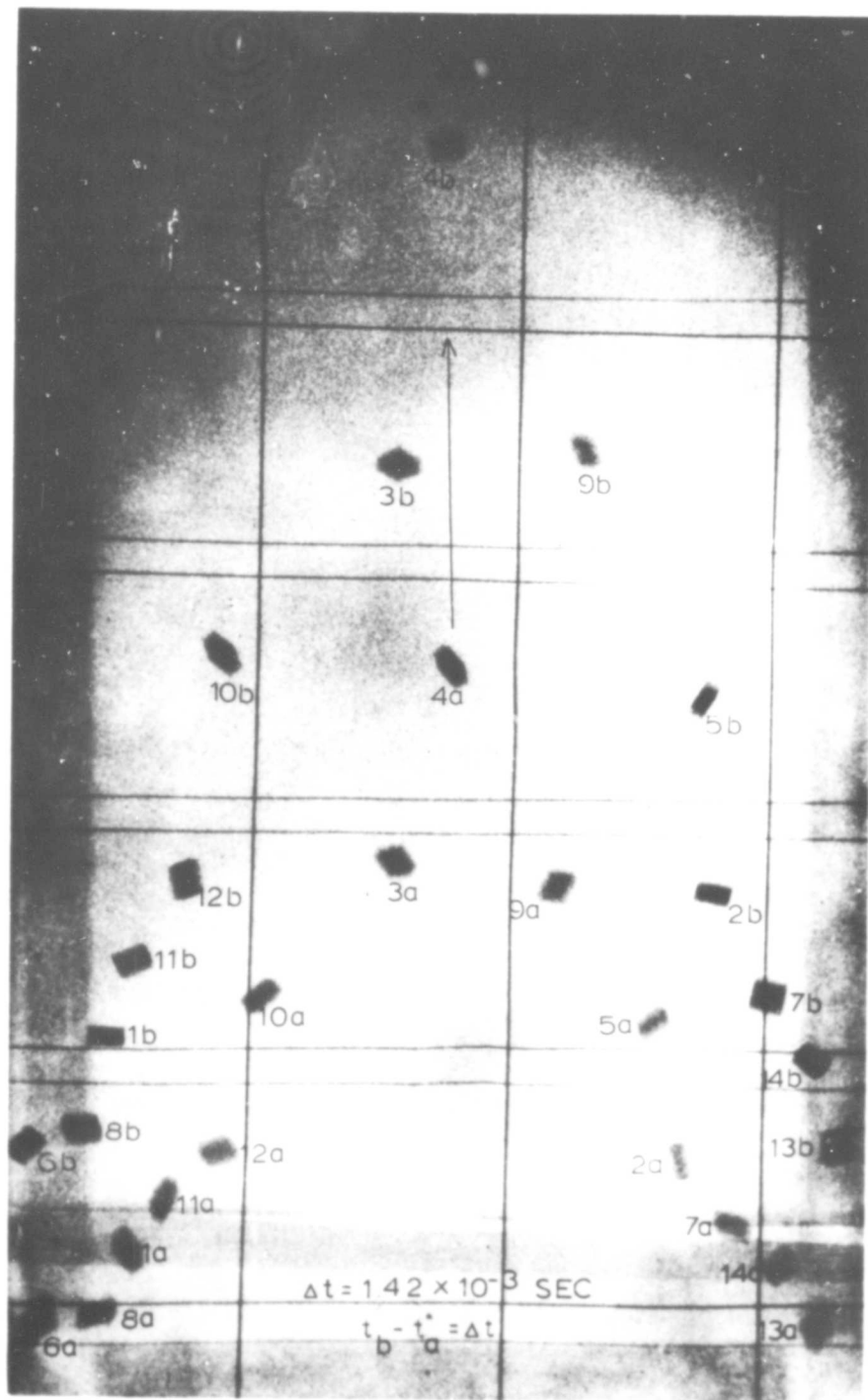


Fig. 17. Sequential Radiograph of Impacted Flyer Plates, AFML Round No. 2406

Plate Number	Distance to Center of Impact (cm)	Initial Mass (mg)	Final Mass (mg)	Velocity (m/sec)	Momentum Intensity (Taps)
13	5.80	327.8	328.4	7.77	633
14	4.90	329.8	329.7	11.49	939
7	3.95	334.1	333.5	14.87	1229
2	3.00	334.5	334.9	20.23	1680
5	2.10	351.5	349.9	27.45	2382
9	1.15	353.6	351.1	41.96	3654
4	.50	356.3	354.0	50.37	4422
3	1.20	354.5	354.3	36.65	3220
10	2.05	353.8	352.1	28.50	2489
12	3.00	340.7	340.3	18.52	1563
11	3.90	335.0	334.3	14.32	1187
1	4.85	331.0	331.6	11.69	961
8	5.80	329.6	329.8	7.88	644
6	6.75	328.5	328.9	5.91	482

Data From Round #2406

Impact of 3.17 mm Cadmium Sphere $V_p = 7.054$ km/sec

Table IV

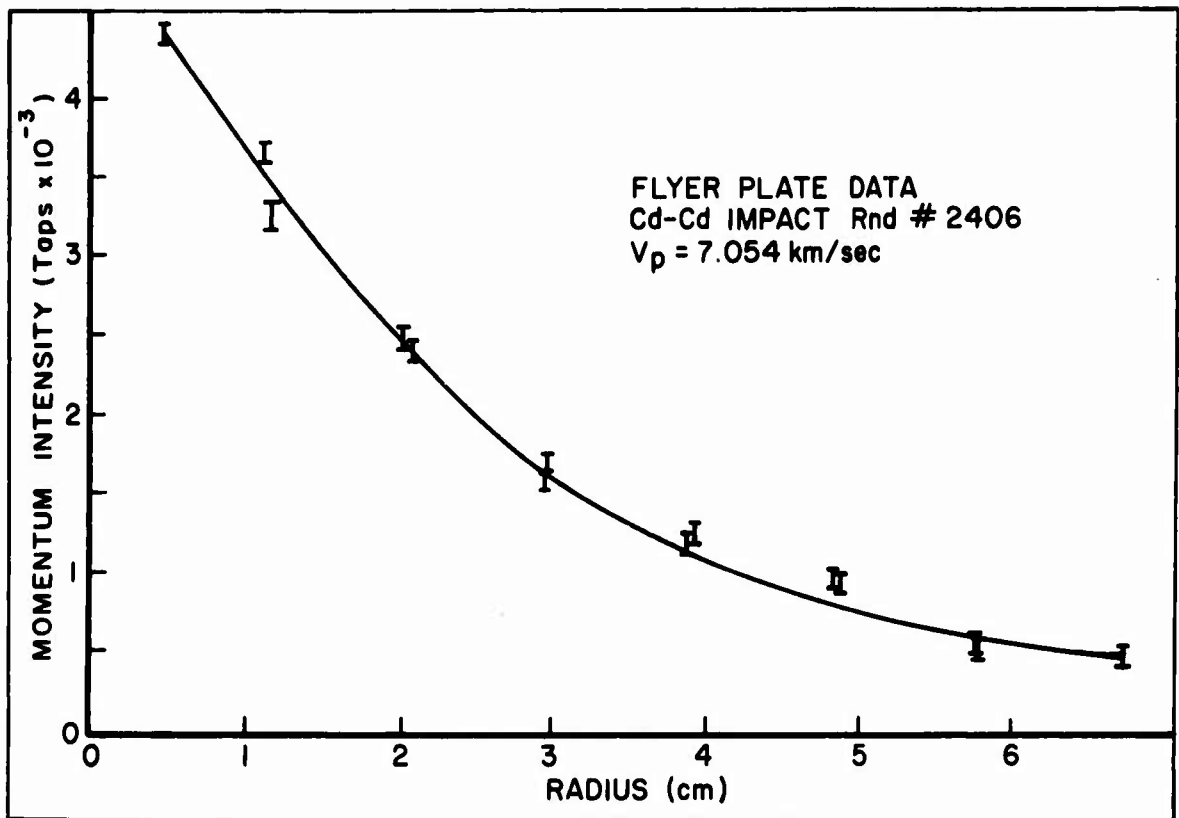


Fig. 18. Momentum Intensity vs Distance to Debris Cloud Center, AFML Round No. 2406

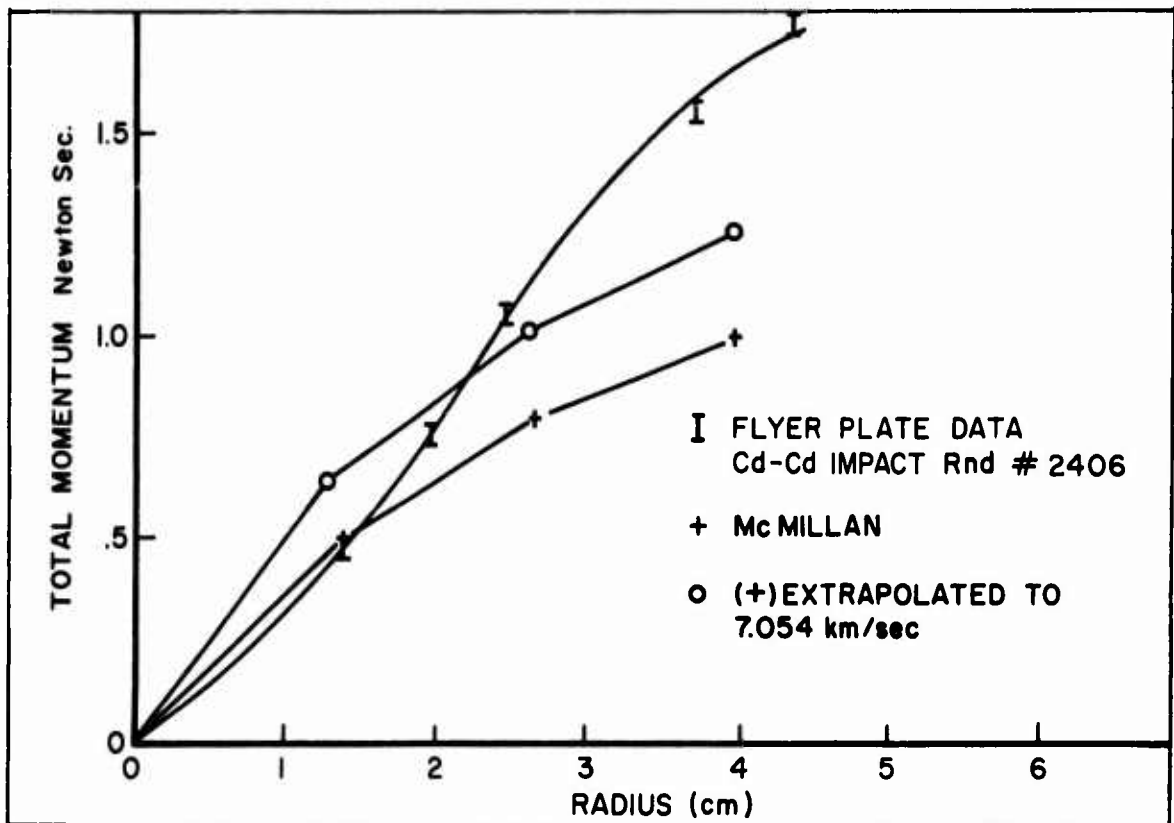


Fig. 19. Total Momentum vs Distance to Debris Cloud Center, AFML Round No. 2406

plating of cadmium on the flyer plates. Some of the flyer plates actually gained mass upon impact. The plates used in the three primary rounds are shown for comparison in Fig. 20.

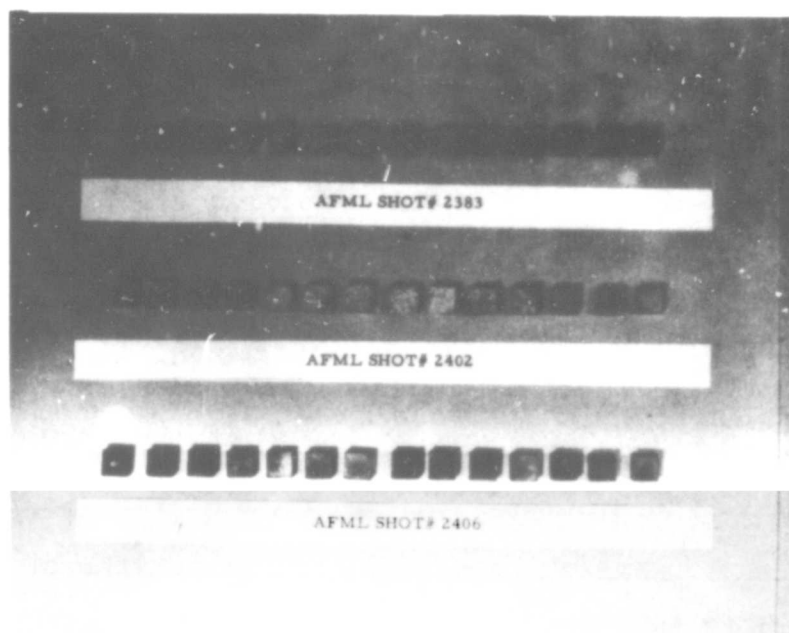


Fig. 20. Photograph of Impacted Flyer Plates

Ballistic Pendulum Measurements

The main objective of the series of experiments with the ballistic pendulum was to determine the internal momentum of the debris cloud itself, i.e. to remove the second momentum multiplication occurring during the cloud interaction with the hull plate. For this to be accomplished, a light pendulum capable of capturing segments of the cloud debris had to be designed and constructed. The data obtained from the flyer plate experiments was used as a basis for determining the allowable mass of the pendulum.

The ballistic pendulum consisted of a fiberglass tube with an inside diameter of 5.7 cm, mounted between two phenolic plates each measuring 7.62 cm x 7.62 cm x .317 cm thick. A third phenolic plate was mounted at the end of the 6-32 threaded steel rods which held the pendulum together. A sketch of the pendulum is shown in Fig. 21. The suspension system consisted of five lengths of radio dial cord attached to a suspension plate shown in Fig. 21. The five wire suspension was a modified version of the six wire suspension used by Gehring (Ref 6: 189). The suspension length of 27 cm was dictated by target tank height restrictions.

The pendulum cylinder was lined with polyethylene as shown in Fig. 22. Polyethylene had been observed in a previous experiment to have the capability of absorbing

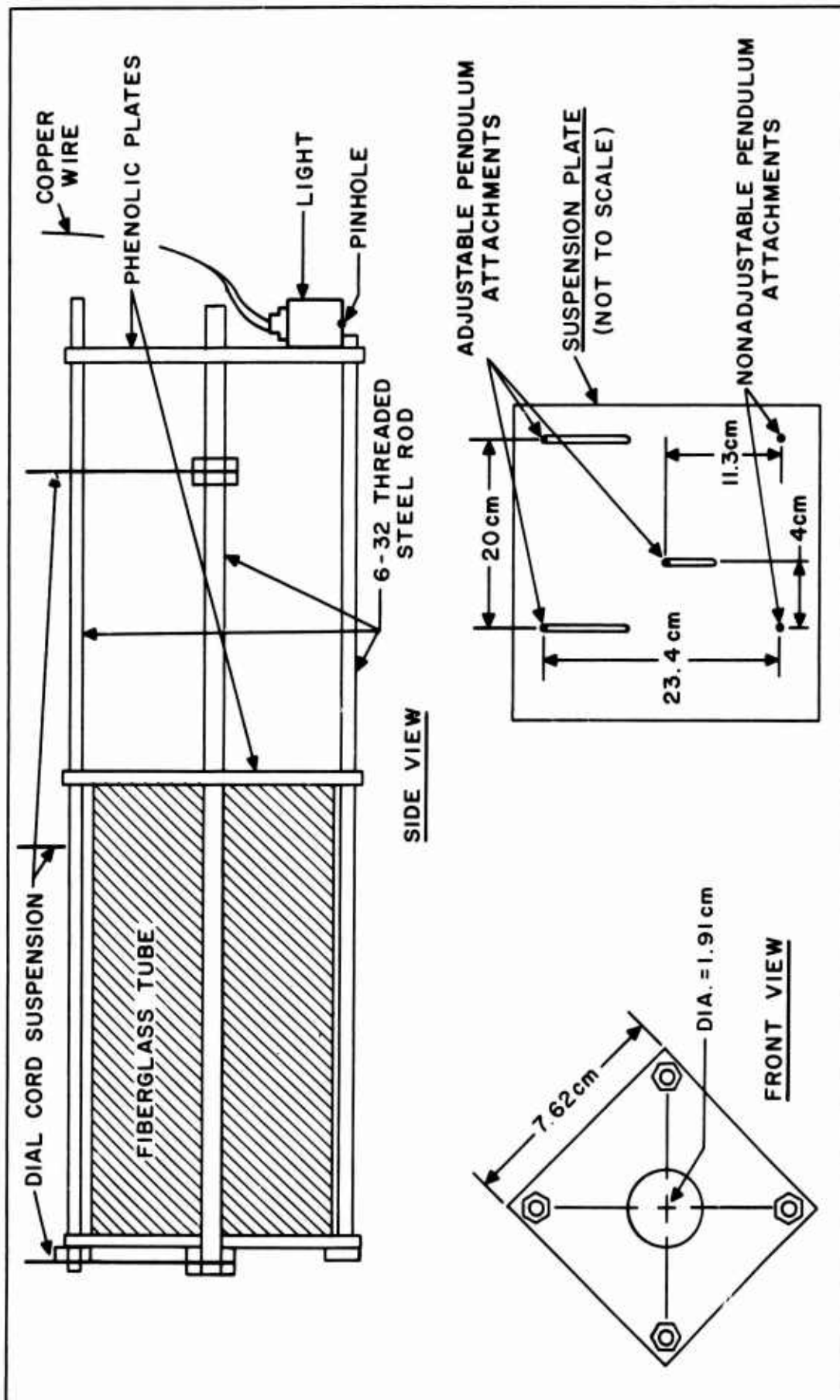


Fig. 21. Ballistic Pendulum Construction

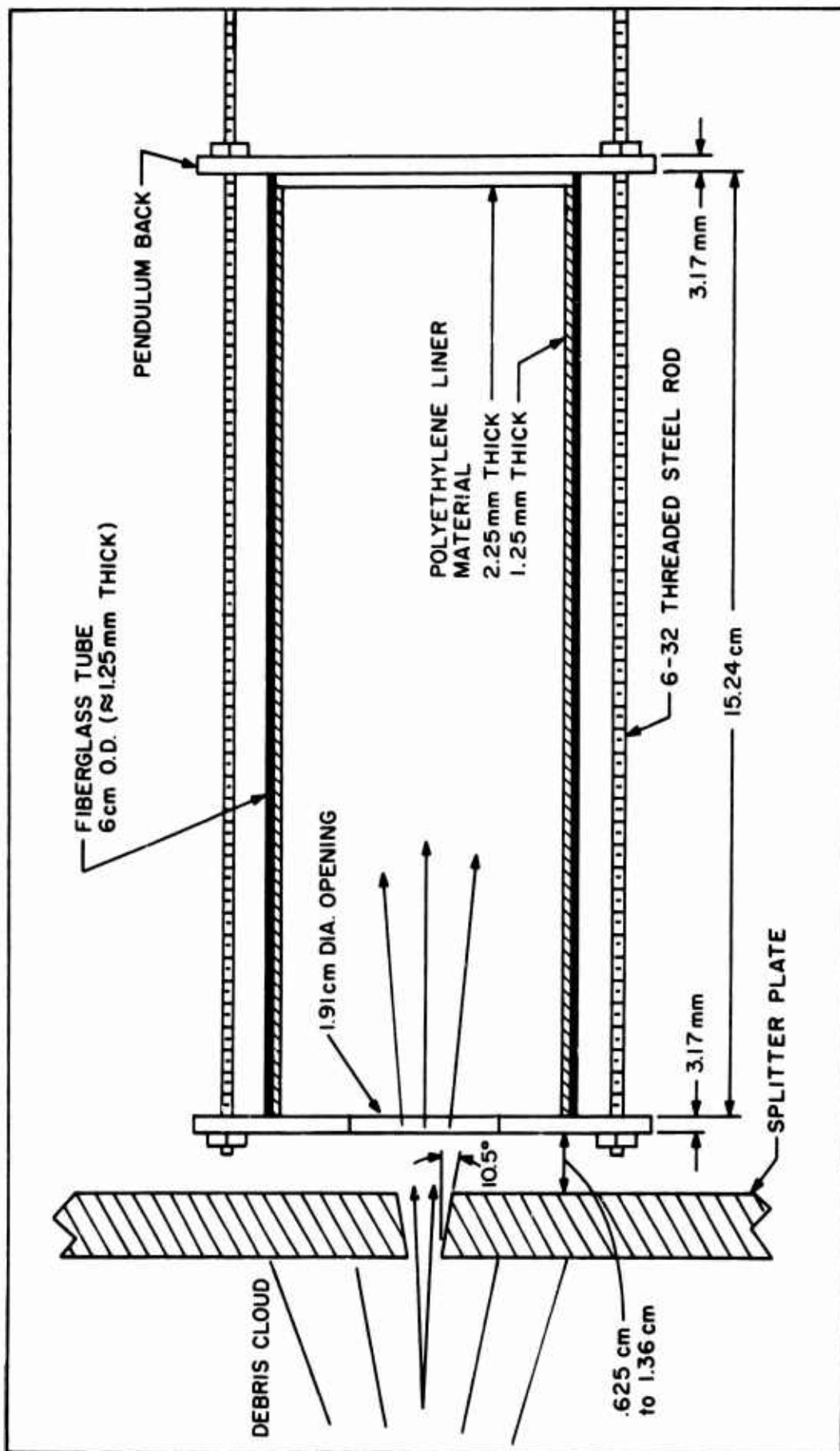


Fig. 22. Ballistic Pendulum Cross Section

cloud debris*. Details of the pendulum and plate attachment methods are shown in Fig. 23. Prior to being placed on the hypervelocity range, the pendulum was calibrated using the air rifle setup shown in Fig. 24. Details of the calibration equipment and procedure are contained in Appendix C. The maximum error encountered with the calibration setup was 4 percent without compensation for pendulum damping.

The ballistic pendulum experiment was setup as shown in Fig. 25. A steel splitter plate shown in Figs. 26 and 27 was set 10.16 cm from the bumper. A movable plate was mounted on the front of the splitter plate in a position to allow a small section of the debris cloud to pass through one of the openings in the splitter plate and into the hollow front section of the pendulum.

The movement transferred to the pendulum was monitored with an open shutter camera and mirror setup depicted in Fig. 25. The camera was positioned (as shown in Fig. 25) so that a view of the bottom point of the rear phenolic plate was obtained. The detail of the mirror, and the view of the camera are shown in Fig. 28. The light source illuminated a reference grid and a .159 cm reflecting aluminum sphere located on the bottom of the rear phenolic plate. The first traces of the reflect-

* Private communication with Mr. P. Denardo of NASA Ames Research Laboratories, Moffett Field, California.

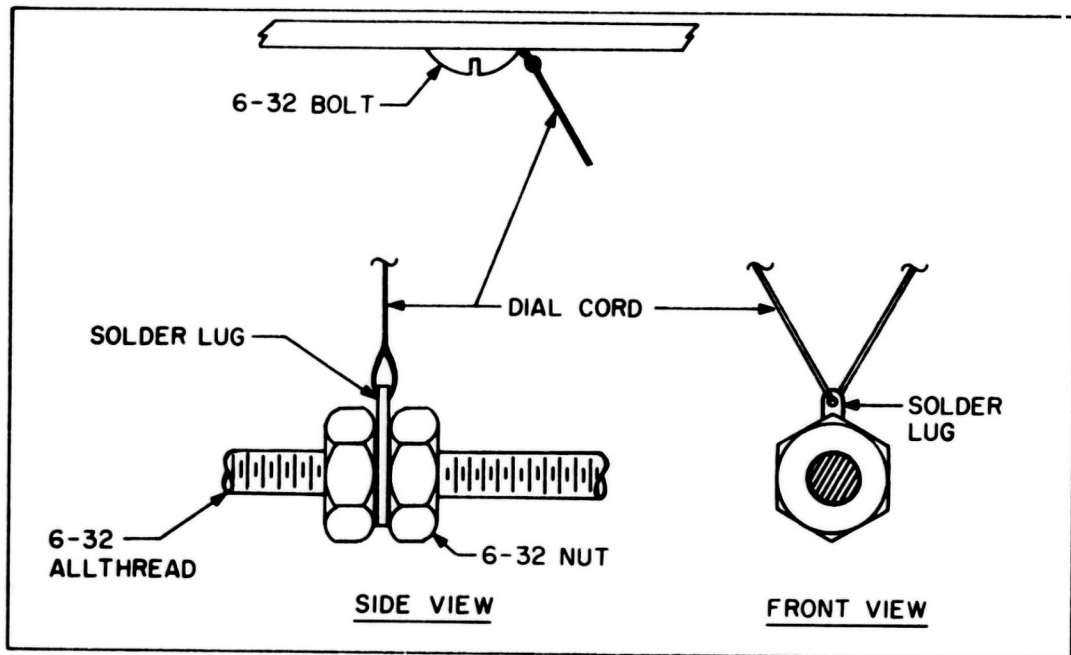


Fig. 23. Ballistic Pendulum Suspension Detail

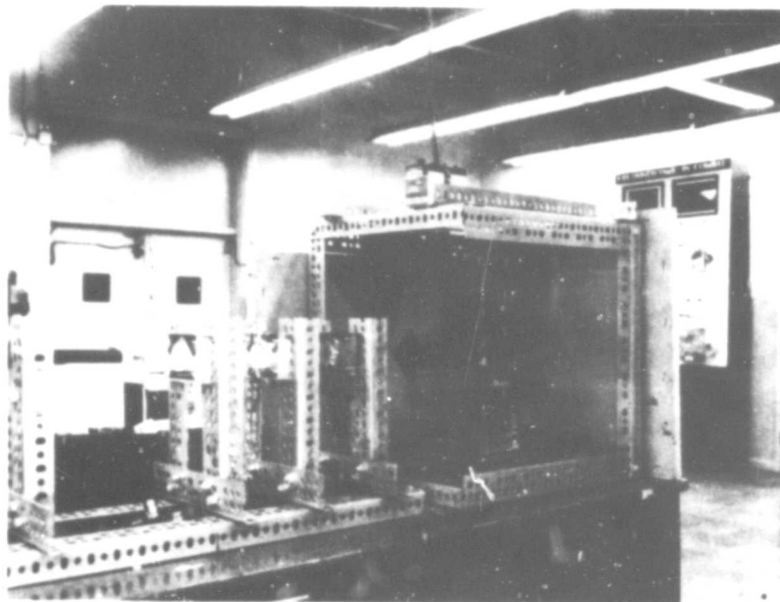


Fig. 24. Photograph of Pendulum Calibration Setup

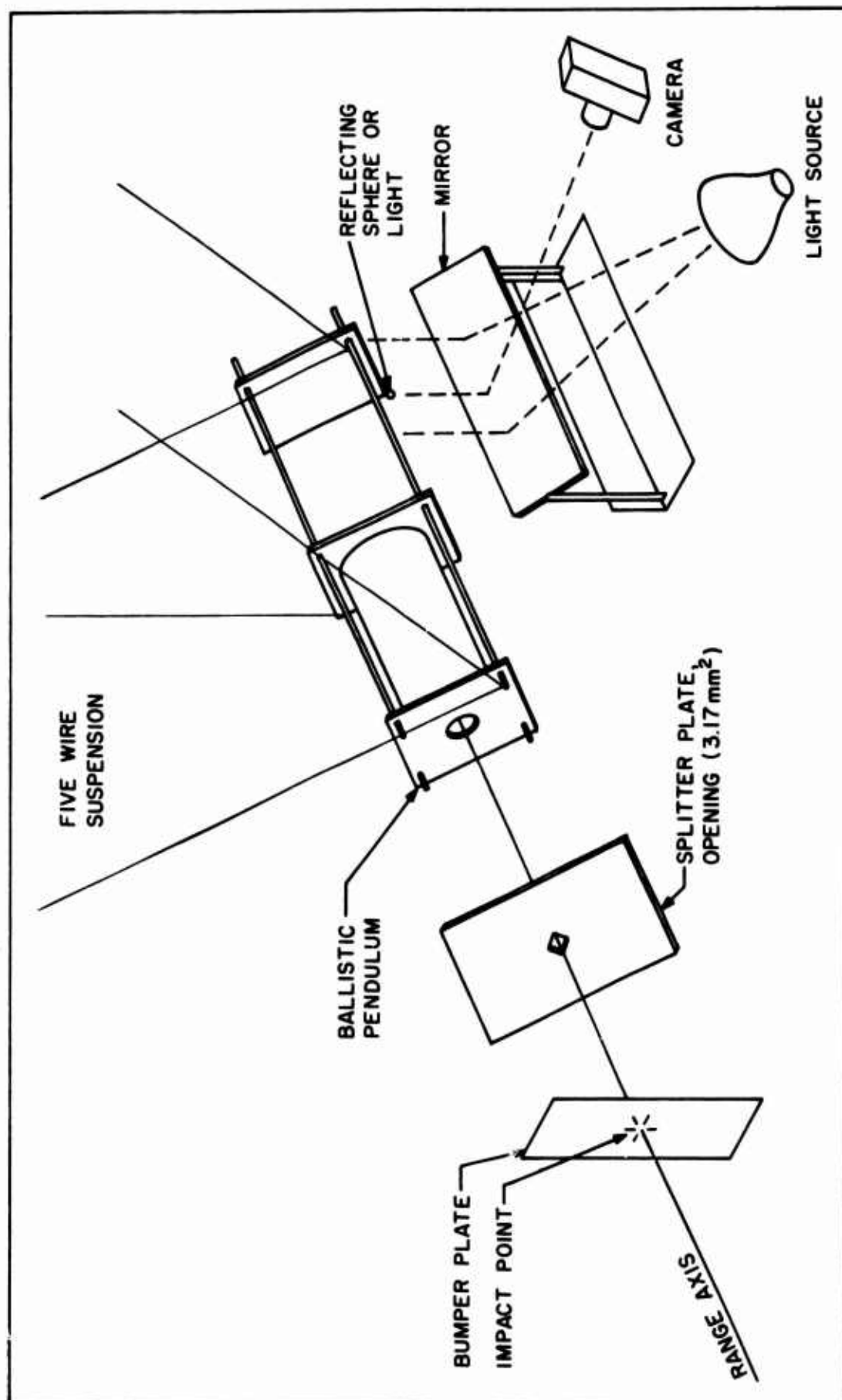


Fig. 25. Ballistic Pendulum Experimental Configuration

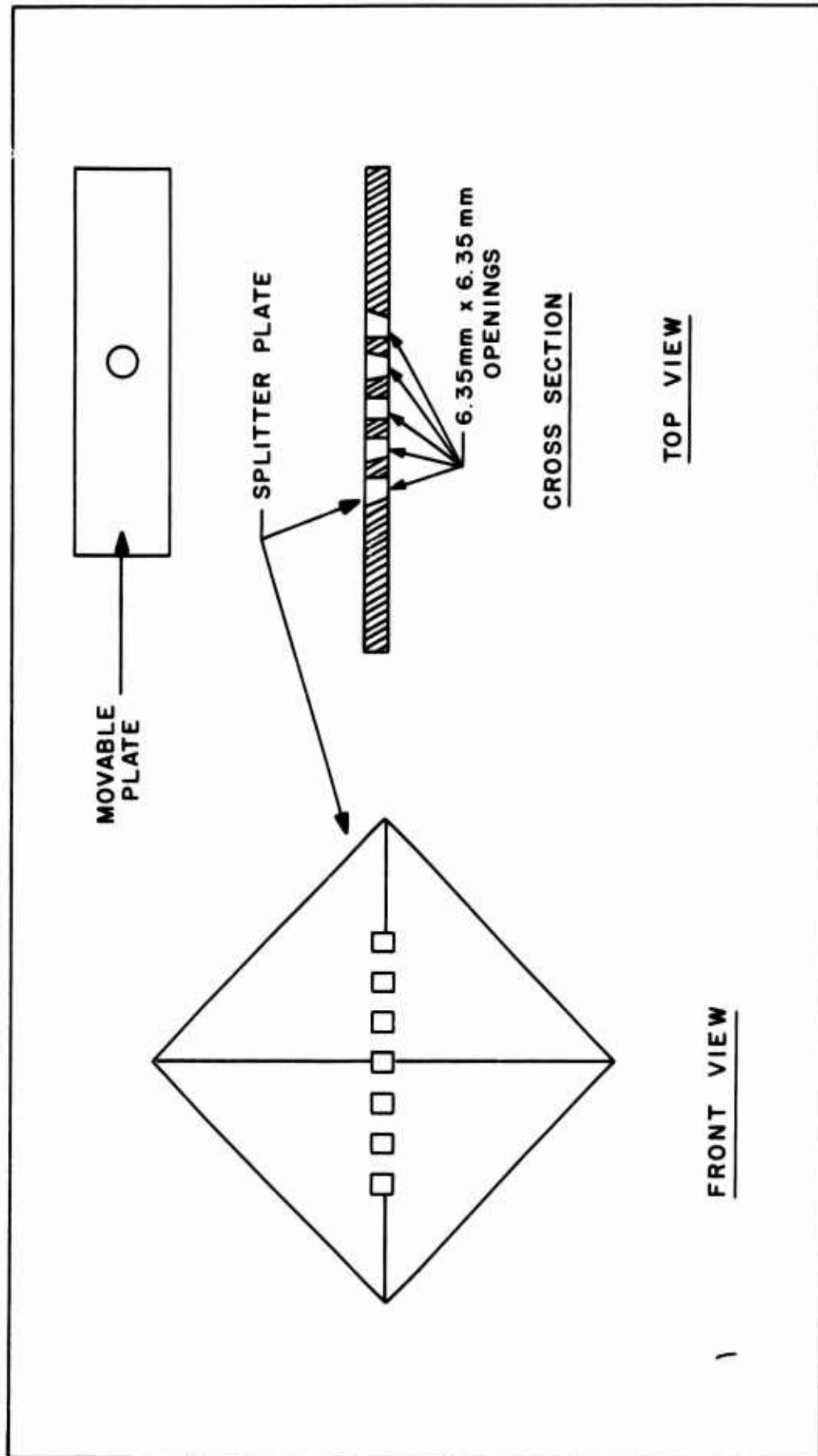


Figure 26. Drawing of Splitter Plate

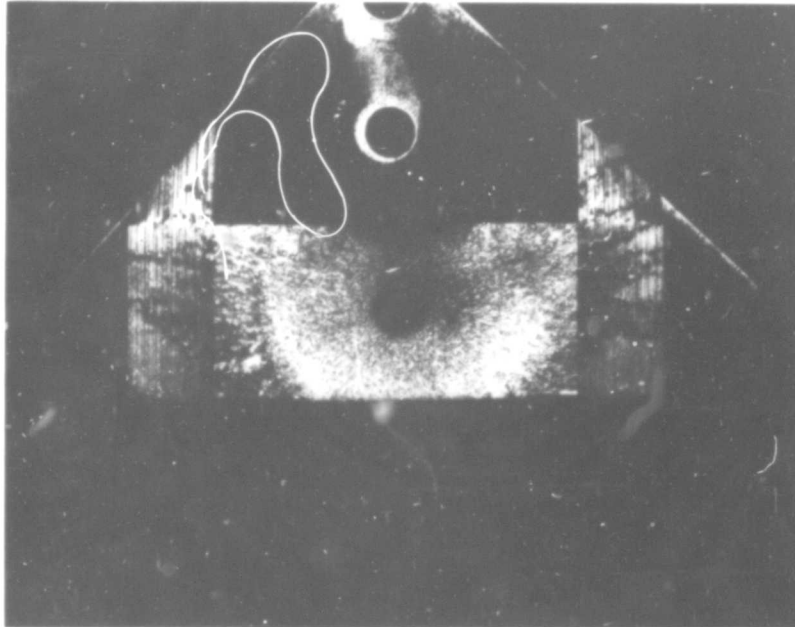


Fig. 27. Photograph of Splitter Plate After Impact:
Movable Plate Attached

ing sphere were faint but could just be analyzed. The situation was improved by substituting a D.C. light source (Mass = 4 gm) consisting of a small light bulb and fine copper wire circuitry for the reflecting sphere on the pendulum.

The reference points used in the reference grid were located at predetermined distances from each other. The horizontal motion of the pendulum was measured using the reference points for determination of the scale. The distance of pendulum movement was determined by comparing the distance moved by the pendulum light source with the known distance between the stationary reference points.

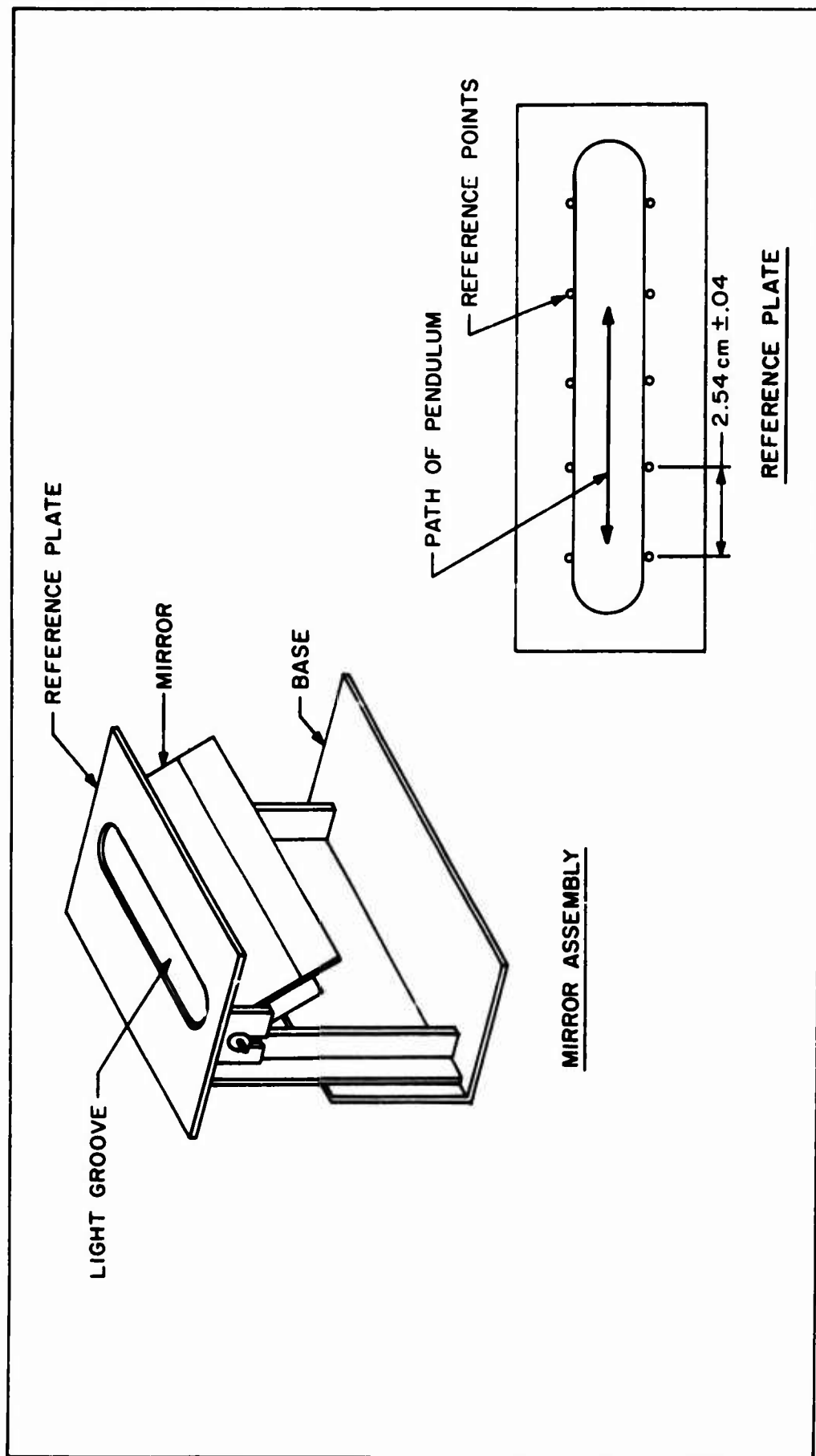


Fig. 28. Detail of Mirror

A film reader capable of resolving one part in 10^4 was used for all measurements.

The basic method for determining momentum imparted to the pendulum from measurements of pendulum motion is to compute the height increase achieved by the pendulum against gravity. The pendulum kinetic energy ($\frac{1}{2} M_I V_I^2$) is equated to the increase in potential energy ($M_I g h$). The required formulation is presented as follows.

The angular motion of the pendulum (θ) is determined from linear pendulum motion using equation (2-4)

$$\sin \theta = \frac{X}{27 \text{ cm}} \text{ where} \quad (2-4)$$

X is the horizontal motion in cm and 27 cm is the suspension length.

The vertical motion (h) is then calculated using equation (2-5)

$$\cos \theta = \frac{27-h}{27 \text{ cm}} \quad (2-5)$$

Once h is known, the initial pendulum velocity and momentum are calculated using equations (2-6) and (2-7)

$$V_I = (2 g h)^{1/2} \quad (2-6)$$

$$P_M = M_I V_I \quad (2-7)$$

where g is the acceleration of gravity (980 cm/sec²),

V_I is the initial velocity of the pendulum and M_I is the pendulum mass.

The measured impulse is not the true momentum

because damping forces are present within the pendulum suspension system that must be accounted for. These forces were evaluated by determining the loss of amplitude per cycle of the free swinging pendulum. Successive values of pendulum amplitudes were determined from timed exposures of several swings of the pendulum (see Appendix C). The losses of amplitude were expressed as percentages. The measured movement of each round constituted only one quarter of a cycle. Thus the average loss per quarter cycle for the magnitudes of horizontal movement measured for each round, must be considered in momentum calculations. For each adjustment made to the pendulum, a new decrement determination was made. This was done to account for any change in the damping forces due to change in the experimental configuration.

Results

The pendulum series was scheduled for three measurements for each of the materials, cadmium, copper, and aluminum. The measurements for each were made for a distance of 0, 1.27 cm, and 2.54 cm from the center of the debris cloud. For each group of three rounds the pendulum was arranged at the appropriate angle to assure passage of the debris into the front cylinder of the pendulum and to assure impact at the rear polyethylene surface.

The experimental results are shown in Fig. 29 and Table V. The images in the first pictures were faint but readable. The third round was an aluminum-aluminum impact with the splitter plate 5.08 cm from the bumper. The results were extrapolated to a 10.16 cm spacing using the method of similar triangles. The momentum intensity at the 10.16 cm spacing was assumed to be one fourth the intensity at 5.08 cm because the intensity varies as the inverse square of the distance. Perforation of the movable plate occurred in Round No. 2468 thus making the measurement of that round suspect. The results are plotted but noted as not fulfilling experimental requirements.

The capture of significant amounts of cloud debris was indicated by close examination of the pendulum polyethylene liner. The debris contained in the pendulum liner was concentrated in the rear section and decreased in amount toward the front of the pendulum cylinder. The inside of the front phenolic plate did indicate that some debris had returned to the front of the cylinder (Fig. 30).

Deviations from a straight line motion can be detected in the pictures of high amplitude swing. These deviations were the result of off-center impact. Analysis of the deviations due to the off center impact indicated that such movements could not be neglected when

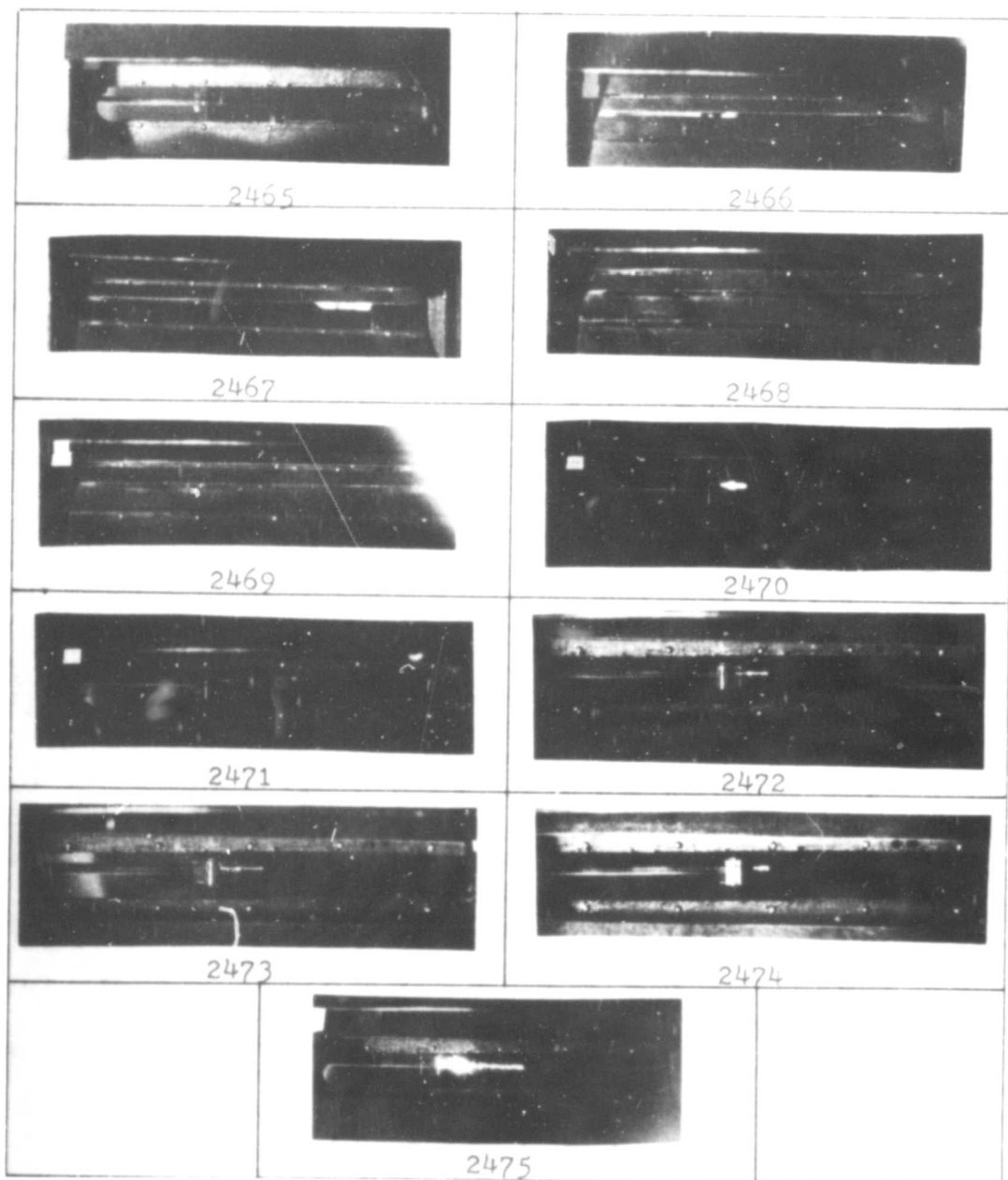


Figure 29

Photographic Results of
Ballistic Pendulum Experiments

Round Number	Distance to Center of Cloud (cm)	Material	Pendulum Motion (cm)	Pendulum Mass (gm)	Momentum gm cm/sec	Corrected for Decrement and Deviation	Normalized to 6.7 km/sec	Momentum Intensity (Taps)
2465	.46	Cu	2.1	228	2879	2946	2970	7378
2466	.34	Cd	2.667	228	3688	3771	3745	9285
2467	.56	Al	1.97	228	2700	2769	2735	1693*
2468	1.67	Cu	1.51	228	2065	2090	2050	5091.4
2469	1.87	Cd	1.98	228	2720	2780	2800	6955
2470	1.50	Al	.461	232	652	698	690	1711
2471	1.60	Cu	1.20	231	1670	1720	1700	4217
2472	2.78	Cu	.635	231	890	932	916	2273
2473	3.29	Cd	.693	231	965	1000	998	2476
2474	2.64	Al	.216	232	291	420	406	1007
2475	.42	Cu	2.50	232	3430	3530	3510	8696

*Extrapolated to 10.16 cm from 5.08 cm

Ballistic Pendulum Results

Table V

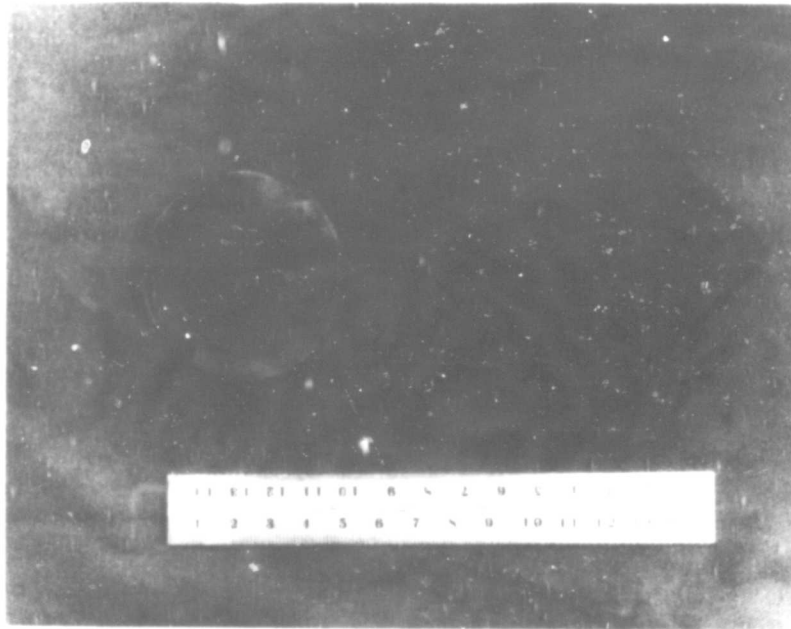


Fig. 30. Photograph of Impacted Polyethylene Plate

compared with the total movement of the pendulum. The analysis (see Appendix C) included direct measurement of the sideward movement using the pendulum calibration system and an impact angle of 90° .

The pendulum setup was constantly under improvement during the course of the experiment. A TV camera was utilized on the last seven rounds to observe possible rebound effects due to pendulum contact with the splitter plate. No rebound effects were observed.

The reflecting aluminum sphere on the rear of the pendulum was replaced by the low mass light source described previously. This was done to obtain a more

positive reading of the pendulum motion. The light source was energized by two dry cell batteries of 3 volts each connected in series. The circuit was made with fine copper wire strung loosely between the light bulb and voltage source. Decrement calculations indicated that the light source and fine copper wire had little effect on the inefficiencies of the system.

A small latch device pictured in Fig. 31 was added to the pendulum system in an attempt to limit the pendulum to one swing. This was done to prevent rewriting of the film record due to any rebound of the pendulum after its first half cycle.

The results of the momentum measurements with the pendulum are presented in Fig. 32. The values presented were normalized to 6.71 km/sec (22,000 ft/sec) for comparison of rounds fired at slightly differing velocities. Normalization was accomplished by multiplying original results by the ratio of 6.71 km/sec to the projectile velocity. This linear treatment is dependent upon the assumption that no unusual phenomena occur over the range of projectile velocities (6.655 km/sec to 6.931 km/sec). The error bars in Fig. 32 indicate possible measurement error.

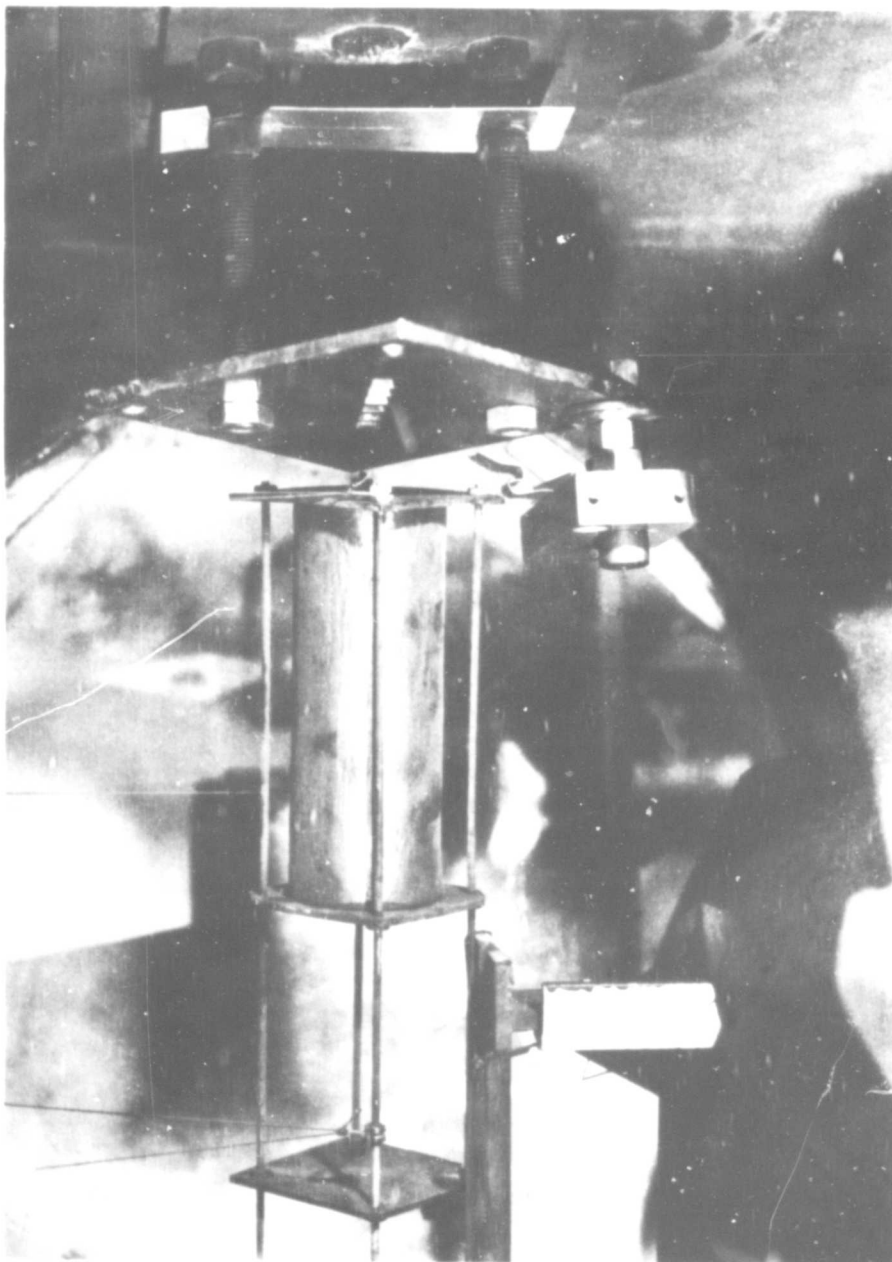


Fig. 31. Photograph of Ballistic Pendulum

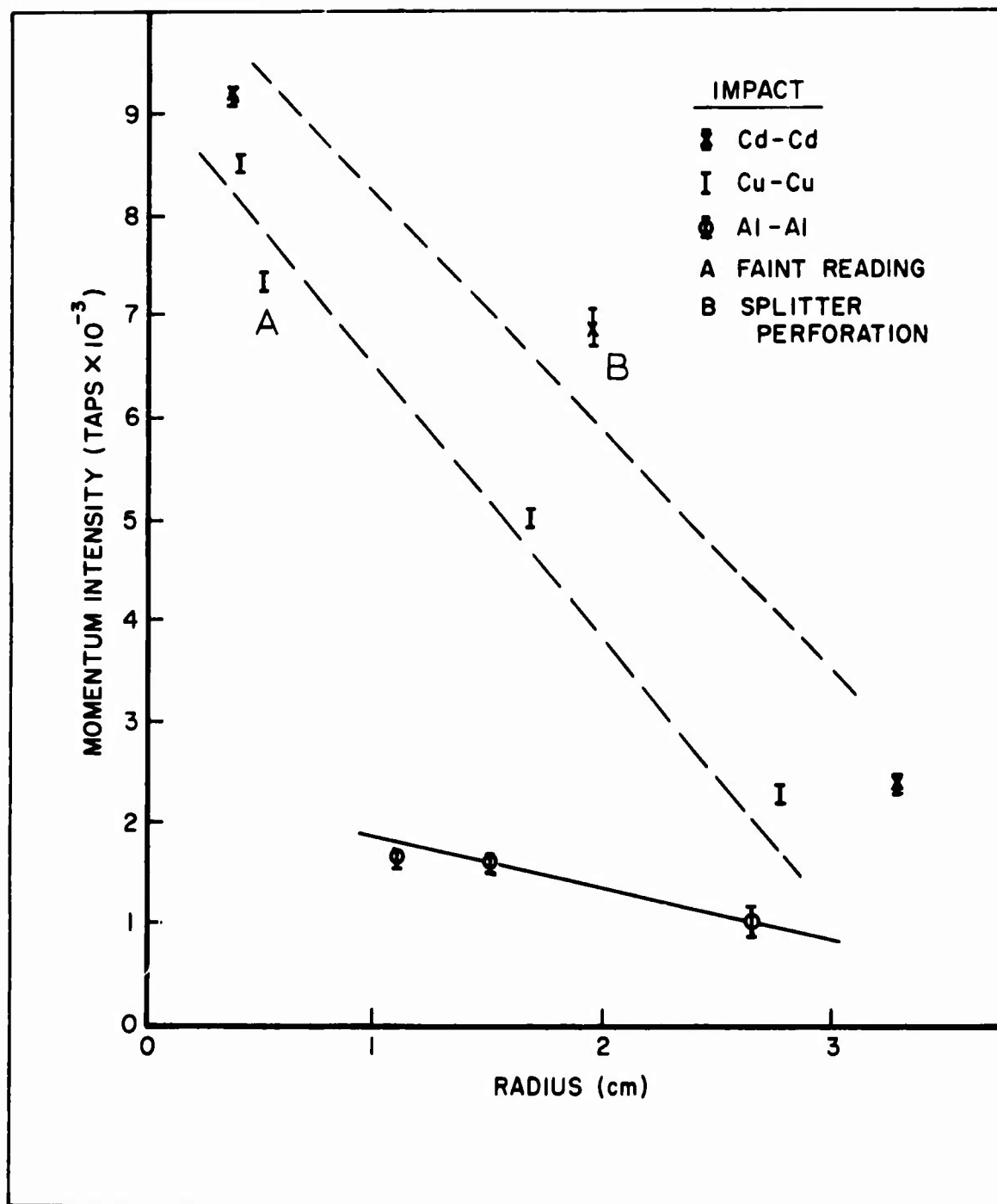


Figure 32

Momentum Intensity vs Distance to Debris Cloud
Center: Ballistic Pendulum Results

III. Discussion of Results and Conclusions

The two phases of the investigation were conducted to determine the debris cloud momentum distribution incident upon the hull plate and the momentum distribution within the debris cloud itself. Observations of simulated hull plate damage from previous investigations have indicated concentrations of damage in the center and on the edge of the center cone of damage. The flyer plate results indicated that the momentum intensity is also concentrated in the center. Concentrations of momentum at the edge of the cloud were not detected. The cadmium cloud, although containing more total momentum than the copper debris cloud, actually possessed less momentum intensity near the center than the copper cloud. This result is reasonable because a more gaseous debris cloud would be expected to spread over a larger area of the hull plate. This result indicates that if higher velocity meteoroids are vaporized by an encounter with an actual spacecraft bumper, the resulting momentum would be spread more evenly over a greater area of the hull plate than previously observed in laboratory simulation experiments. This does not mean that the highly vaporized cloud is not damaging. The total momentum multiplication factor could be in excess of two for vapor generating impacts indicating that the hull plate would be subjected to a dispersed momentum of twice the momentum of the incoming projectile. The total momentum multiplication

factor is the result of two multiplication effects. The first momentum multiplication effect results from the impact of the projectile on the bumper. The second multiplication effect results from the reflection of debris and cratering resulting from the interaction of the debris cloud and hull plate. A multiplication factor greater than two will occur when the gaseous debris cloud is almost totally reflected by the hull plate. The first multiplication factor is relatively small as indicated by the low velocity and small amount of the upstream debris. The hull plate multiplication effect caused by a gaseous cloud would be the major contribution to the overall multiplication factor of 2 since it would multiply a momentum already somewhat greater than the incident momentum.

Comparison of the flyer plate results with Carey's momentum calculations was possible for only one material, copper. The crater volume - energy method of calculating momentum could not be used for cadmium because of the fine cratering and gaseous composition of the debris cloud. Data from Round No. 2383 and Carey's data (Ref 3: 49) are presented in Fig. 33. The data points represent the momentum within circular sections of the debris cloud, with each data point at the center of the section. The similarities and differences in the two experiments must be noted in any realistic comparison of the two. The projectile and bumper materials and the projectile size and shape were identical. The bumper used in Carey's

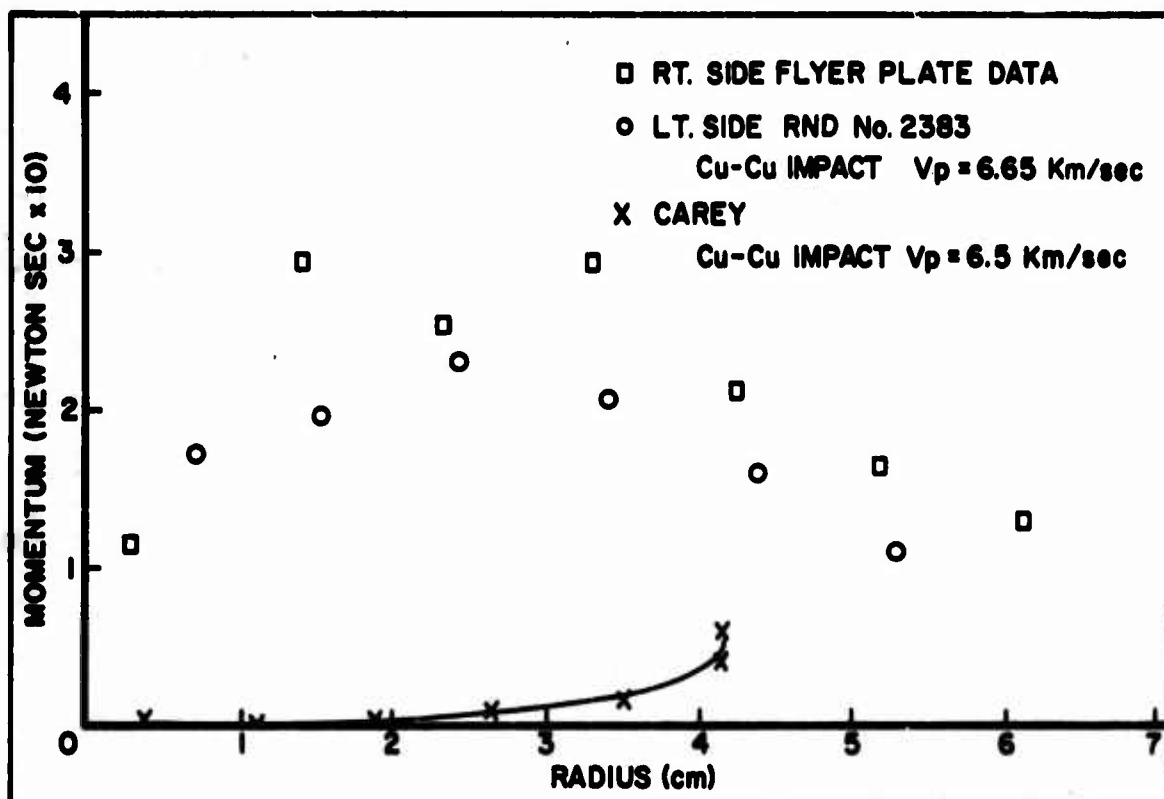


Fig. 33. Flyer Plate Data Compared With Results of Crater Volume - Energy Calculation

experiment was 1.59 mm thick as compared with the 0.79 mm thick bumper used in Round No. 2383. A detailed and exact comparison of the flyer plate results with Carey's calculations is not possible because of the differences in experimental parameters and measurement techniques. The thicker bumper plate used by Carey absorbed more energy and momentum than the thinner bumper plate used in Round No. 2383. Because of the vapor and liquid composition of the highly shocked center section of the debris cloud Carey's readings for the center of the cloud were not indicative of the actual momentum. The differences in results indicate that the crater volume - energy method

is not valid for the calculation of the debris cloud energy and momentum in vapor and liquid generating impacts.

The flyer plates suffered differing degrees of damage depending upon the material impacted. The flyer plates impacted by the cadmium debris cloud were plated with cadmium with the impacted surfaces showing signs of very fine craters. The mechanism for hull plate failure caused by a gaseous debris cloud such as cadmium would be buckling and eventual rupture due to the high pressures within the cloud.

Preliminary determination of the expected pendulum results indicated that the pendulum would measure less momentum than that measured by the flyer plates for corresponding points within the debris cloud. This was found not to be the case. The ballistic pendulum measurements were consistently greater than those of the flyer plates as shown in Figs. 34, 35, and 36. The differences between expected and actual results could not be explained as measurement error.

The suspected sources of error were accounted for with adjustments to the measured value made as determined by the decrement calculations. The analysis of the pendulum motions due to off center impact indicated that they were significant when compared with the total measured momentum (see Appendix C). The momentum lost to sideward motion was calculated from the deviation

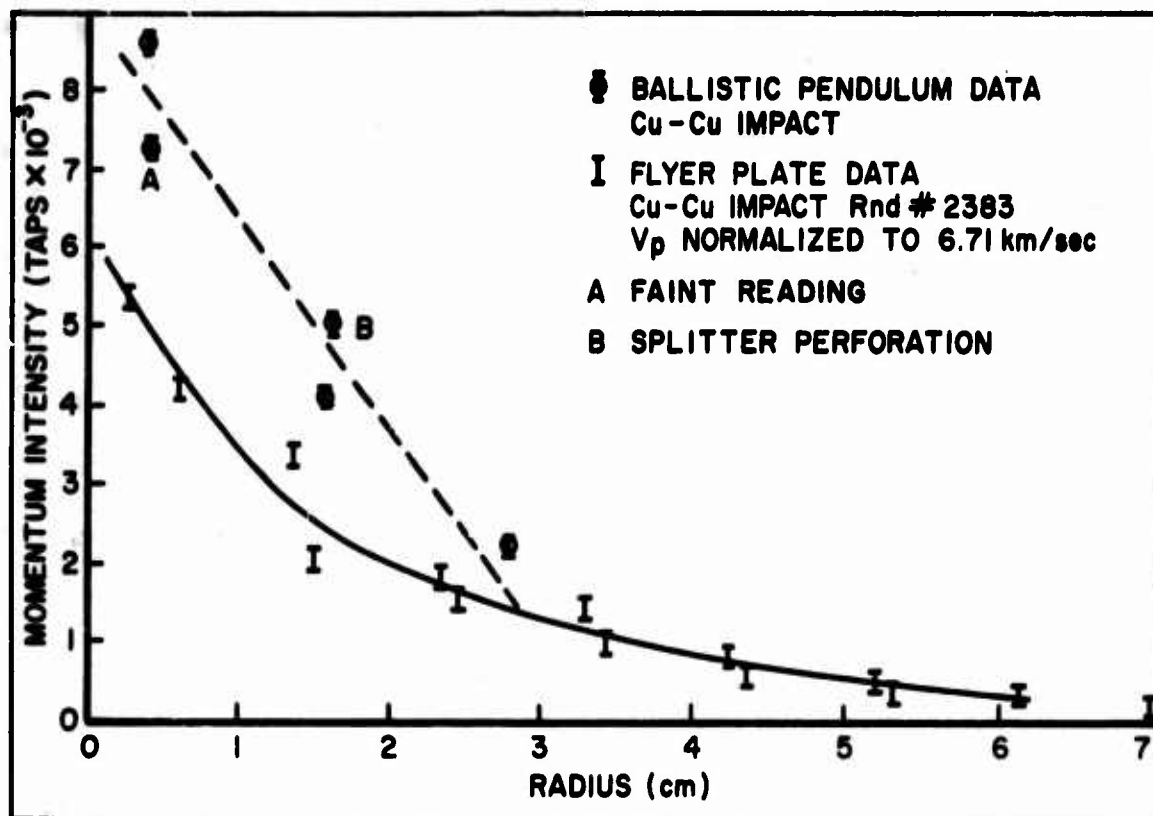


Fig. 34. Comparison of Flyer and Pendulum Data: Copper Impact

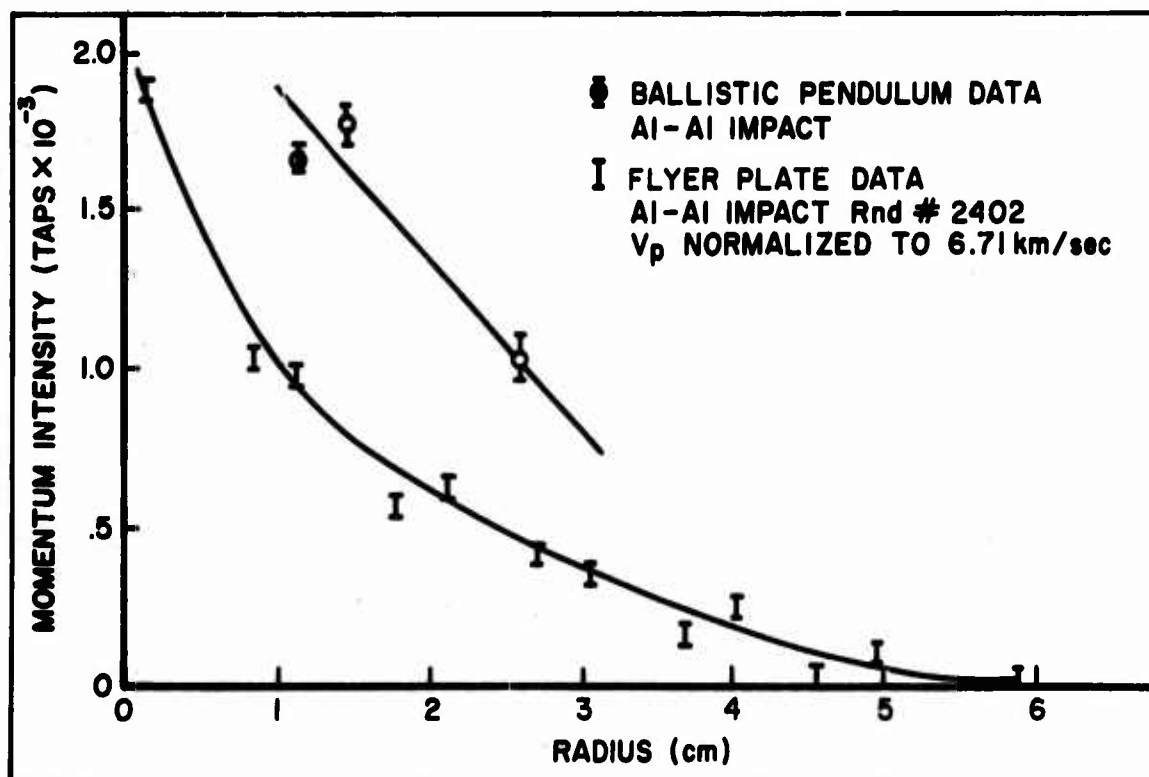


Fig. 35. Comparison of Flyer and Pendulum Data: Aluminum Impact

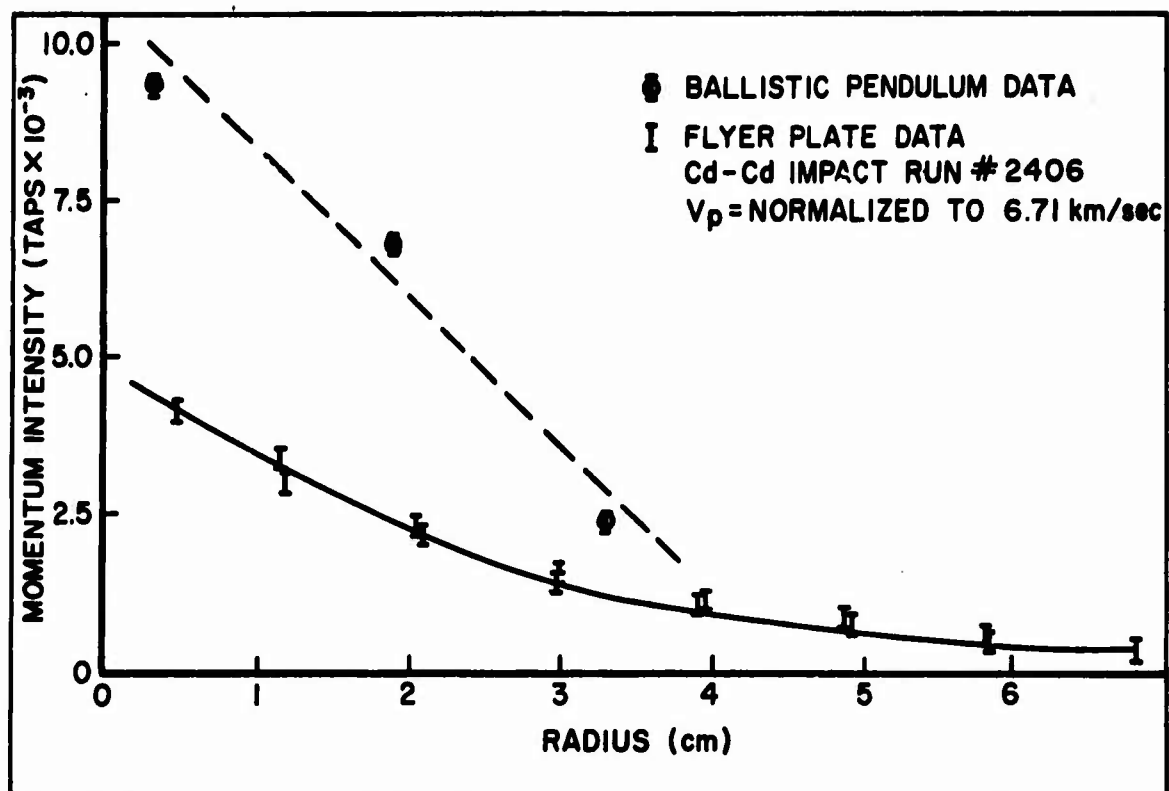


Fig. 36. Comparison of Flyer and Pendulum Data: Cadmium Impact

measurements and the results were adjusted accordingly.

The discrepancy between expected and obtained results was first recognized after three rounds were conducted with the pendulum oriented along the range axis. Examination of sequential photographs of a previous cadmium impact (Round No. 2427, $V_p = 7.029$ km/sec) yielded a possible explanation (see Fig. 37). A late time jetting of debris was observed at 20.8 μ sec.

The late jetting of debris is believed to be the result of the cloud confinement phenomenon associated with the bumper-hull plate system. The cloud confinement phenomenon is defined as the continued accumulation of debris along the surface of the hull plate and an apparent confinement of the debris within the final cloud dimension. This phenomenon had been observed in previous experiments but had not been fully investigated. In Fig. 37, the buildup of the debris after the debris cloud has reached its maximum diameter can be observed. This buildup of debris caused by the continued influx of debris results in an increase in cloud pressure toward the center causing the eventual late jetting. The mechanism causing the confinement of the cloud is not known. It had been observed and is proposed as the cause for the resulting high pendulum measurements. The consequence of the confinement phenomenon is that the hull plate will experience a longer impulse than previously expected. The exact nature of this phenomenon remains to be investigated.

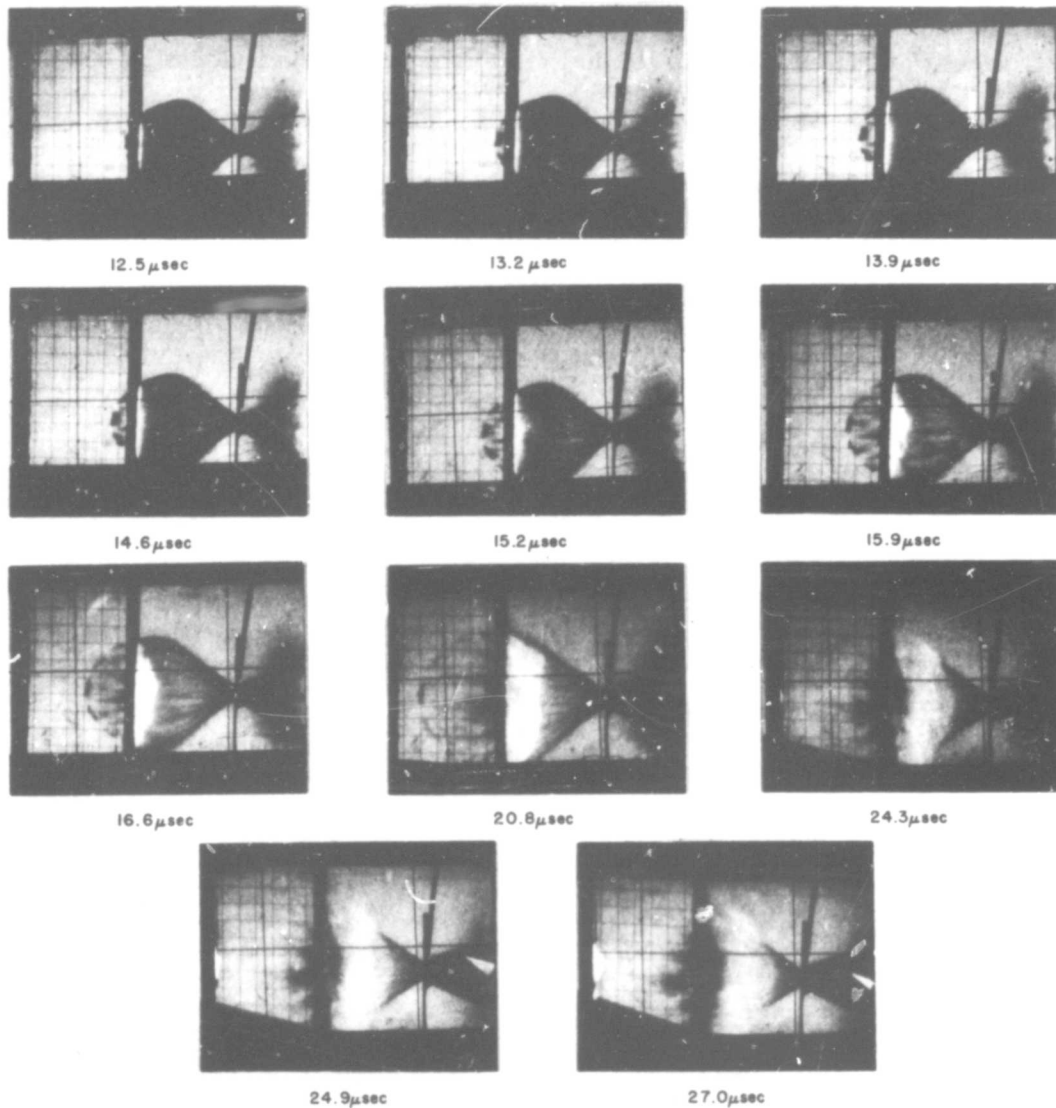


Figure 37

Sequential Photographs of
Cloud-Splitter Interaction

The results of the pendulum experiment indicate that the unconfined debris cloud and the confined debris cloud have different momentum intensity distribution. Thus any knowledge of the properties of the debris cloud itself, must be considered in relation to its reaction with the hull plate.

Two alternative explanations for the unexpected pendulum results were considered and dismissed as more experimental work was completed. The possibility of a rebound effect from the pendulum impacting the splitter plate was definitely eliminated. Observations of the pendulum during impact showed no such effect.

The possibility of debris and a blast from upstream following the projectile and imparting an additional momentum to the pendulum was also considered. The baffles in the blast tank and closure of the sabot plate should have prevented any such effect. The fact that the high readings were present at points off the range axis indicated that this did not occur. The bumper plate would intercept most of this debris.

From these observations and the results of both experimental phases the following conclusions were drawn:

(1) The unexpectedly high momentum measurements provided by the ballistic pendulum experiment were caused by the debris cloud confinement phenomenon. The continued interaction of the debris cloud with the splitter plate resulted in the late time jetting and the additional measured

momentum. (2) The momentum measured by the ballistic pendulum realistically reflects the momentum distribution in the confined debris cloud because of the elimination of the second multiplication effect. The hull-plate would thus experience a momentum intensity greater than that measured with the pendulum. (3) The flyer plates measured the momentum distribution of the unconfined debris cloud including the multiplication effect due to flyer plate cratering. The flyer plate results represent a high estimate of the actual momentum intensity distribution within the debris cloud. The elimination of the second multiplication effect in the flyer plate experiment would allow the measurement of the actual momentum distribution within the unconfined debris cloud.

IV. Recommendations

The investigation of the cloud momentum distribution should be continued after adjustments have been made in the experimental techniques. The recommended adjustments are the following: (1) Flyer plates should be used in conjunction with a splitter plate to measure the momentum incident upon the hull plate. Flyer plates mounted behind a splitter plate, but not in contact with it, would experience both multiplication effects and the late time jetting. Results could be compared to the already obtained pendulum results to determine the second multiplication effect caused by cloud confinement. (2) A specially designed splitter plate should be constructed for use with the ballistic pendulum. If constructed properly, it could funnel a cloud segment of interest back to the pendulum while deflecting the remaining debris to only a slight degree. An inverted funnel shaped splitter would divert the debris away from the splitter opening and eliminate the reading of late jetting. These measurements could then be compared with the flyer plate measurements presented in this report to isolate the second multiplication effect. (3) A piezoelectric pressure sensing bar (Ref 5: 28) can be used to obtain pressure versus time profiles at various points within the debris cloud. This pressure bar could be mounted in a hull plate for measurement of the pressure pulse due to cloud confinement. It could also

be used with the previously mentioned funnel device to measure the unconfined cloud pressure. (4) The configuration of the pendulum should be modified. The use of a longer tube would insure entrapment of more of the debris cloud. An improved permanent mounting arrangement would add to the accuracy and flexibility of the pendulum system. The use of a six wire suspension would allow easier analysis of sideward pendulum motion. A lighter pendulum should be constructed for further investigation of the extremes of the debris cloud. The pendulum used in this investigation proved to be of more than sufficient strength to withstand the debris cloud impact, thus indicating the practicability of a pendulum with less strength. (5) The addition of another camera to monitor the center section of the pendulum may be advisable. The exact relative motions of different points on the pendulum could then be observed for use in corrections for off-center impact.

Bibliography

1. Bjork, R.L., K.N. Kreyenhagen and M.H. Wagner. Analytical Study of Impact Effects as Applied to the Meteoroid Hazard, NASA CR-757. Sherman Oaks, California: Shock Hydrodynamics Inc., May 1967.
2. Burton, Ralph. Vibration and Impact, Reading, Massachusetts: Addison Wesley Publishing Co. Inc., 1958.
3. Carey, Donald A. An Investigation of the Debris Cloud Produced by the Impact of Spheres on Thin Sheets, Thesis: Wright-Patterson Air Force Base, Ohio: Air Force Institute of Technology, 1967.
4. Dozier, James B. Meteoroid and Hypervelocity Impact Physics Research at MSFC, NASA N67-30612. Huntsville, Alabama, 1967.
5. Friend, W.H., C.L. Murphy and I. Stanfield, Review of Meteoroid-Bumper Interaction Studies at McGill University, NASA CR-54857 (SRI-R-15). Montreal Canada: Space Research Center, McGill University, August 1966.
6. Gehring, J.W., C.L. Meyers and J.A. Charest. "Experimental Studies of Impact Phenomena and Correlation with Theoretical Models", Proceedings: Seventh Hypervelocity Impact Symposium, Vol V, February 1965.
7. Maiden, C.J. "Meteoroid Impact" in Space Exploration edited by Donald P. LeGalley and John W. McKee. New York: McGraw-Hill Book Co., 1964.
8. McMillan, A.R. Experimental Investigations of Simulated Meteoroid Damage to Various Space Structures NASA CR-915 Santa Barbara, California: General Motors Corporation, January 1968.
9. Olshaker, A.E. and R.L. Bjork. "Hydrodynamics Applied to Hypervelocity Impact", "The Role of Melting and Vaporization in Hypervelocity Impact" Proceedings: Fifth Symposium on Hypervelocity Impact Symposium, Vol I Part 1, April 1962.

10. Swift, H.F. The Air Force Materials Laboratory Hypervelocity Ballistics Range, AFML TR-67-2 Wright-Patterson Air Force Base, Ohio: Air Force Materials Laboratory, 1967.
11. Taylor, Angus E. Calculus and Analytic Geometry, New Jersey: Prentice Hall Inc., 1959.
12. Thomson, William T. Mechanical Vibrations, New York: Prentice Hall Inc., 1948.

Appendix A

Description of Equipment

The facilities of the Air Force Materials Laboratory Hypervelocity Ballistics Range were used for this experimental investigation. The main items of equipment used included the light-gas gun, streak camera winker system, and flash x-ray equipment. A description of the ballistics range and equipment is contained in Reference 10. A brief description of the equipment used is contained in this appendix.

AFML Light-Gas Gun

The AFML light-gas gun is shown in Fig. 38. The gun uses a 40 mm MK4 piston loaded cartridge as the propellant device and is fired with a remote-control, electrical solenoid firing pin. The operation sequence is shown schematically in Fig. 39.

As the propellant is ignited, the piston is forced forward compressing the hydrogen gas. (Initial pressure 18.7 bars) When the hydrogen gas reaches a sufficiently high pressure a shear disc is ruptured. The projectile is mounted in the front of a cylindrically shaped plastic sabot which fits snugly into the barrel. The sabot is then forced through the barrel by the expanding gas and attains very high velocity. After the sabot enters the blast tank it is separated from the projectile by the

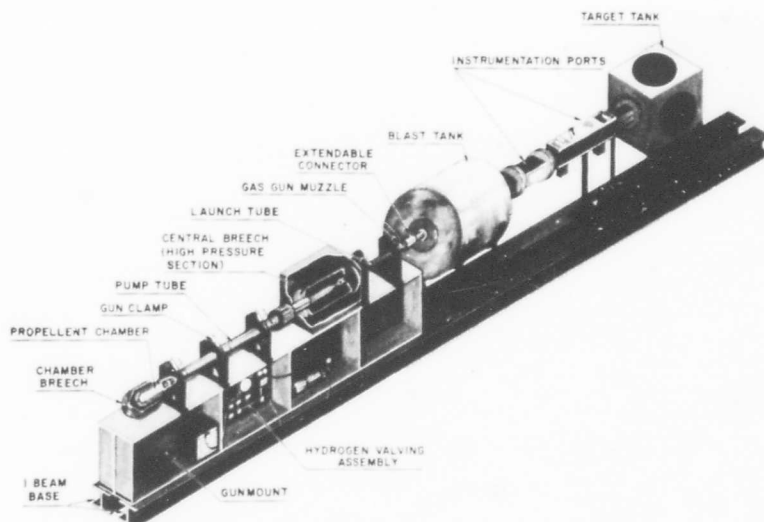


Fig. 38. AFML Light Gas Gun

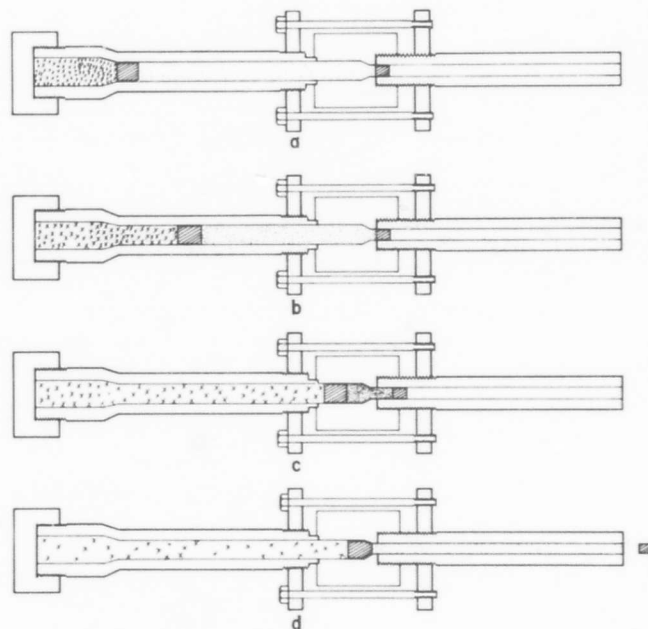


Fig. 39. Light Gas Gun Firing Sequence

aerodynamic forces of the 25 torr pressure in the range. The projectile then proceeds through a small opening downrange to impact. A special sabot impact plate forms the small opening which is closed by the impact of the sabot thus preventing air blast and debris from following the projectile downrange.

Projectile velocity and condition are monitored prior to the impact with camera systems for velocity measurement and the assurance of projectile condition.

Targets used for impact studies are mounted in the target tank located at the end of the range. The target tank is constructed as a (60.8 cm x 60.8 cm x 60.8 cm) steel cube with five circular (dia. = 40.6 cm) access ports. These ports are used for target support and observation.

Streak Camera Winker System

The streak camera winker system is shown schematically in Fig. 40. This system is used for determining relative event times and projectile velocity. The film velocity of the camera is known thus allowing time calculations for events registered on the film to be made. The xenon winker tubes can be triggered by impact associated events so that their relative times can be established.

Image Converter Camera System

High speed image converter cameras* are used for measuring size, shape and velocity of projectiles in flight. The cameras are located along axes that are perpendicular to both the range axis and each other for the accurate determination of projectile trajectory and velocity

Each camera is triggered with an ion switch which is discharged by the presence of the ionized gas sheath surrounding the launched pellet.

Flash X-ray System

Two 150 kv flash x-ray systems with 30 nanosecond pulse duration* were used in the experiment. The capabilities of these x-ray units are detailed in Reference 10.

Contact Switches

The contact switches used for the pendulum calibration and for triggering of the flyer plate experiments were identical in principal. A voltage is applied across a mylar insulation located between two strips of aluminum foil. Once the insulation is broken, an arc closes the switch which registers a xenon flash on the streak camera film. The switches themselves were made with one strip of mylar clamped between foil strips which were connected,

*Beckman & Whitley Image Converter Camera Model 500.

*Field Emission Corporation Model 231.

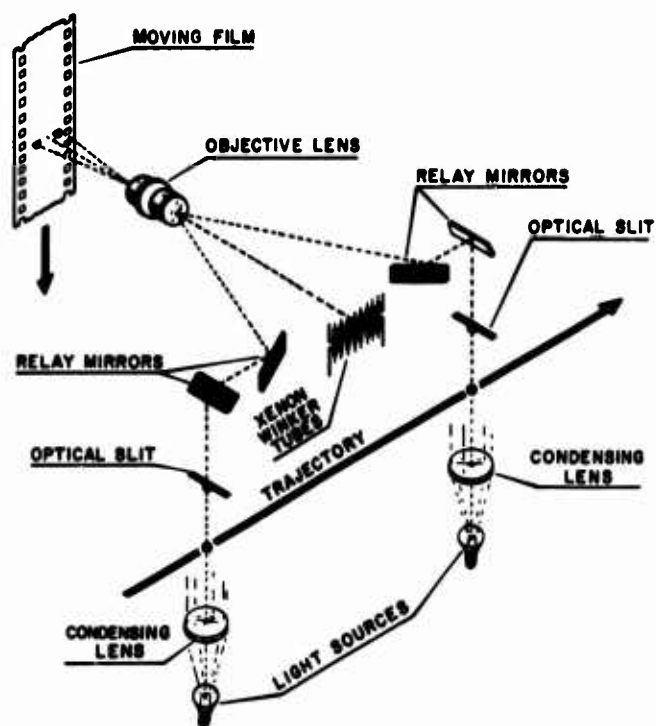


Fig. 40. Streak Camera Winker System

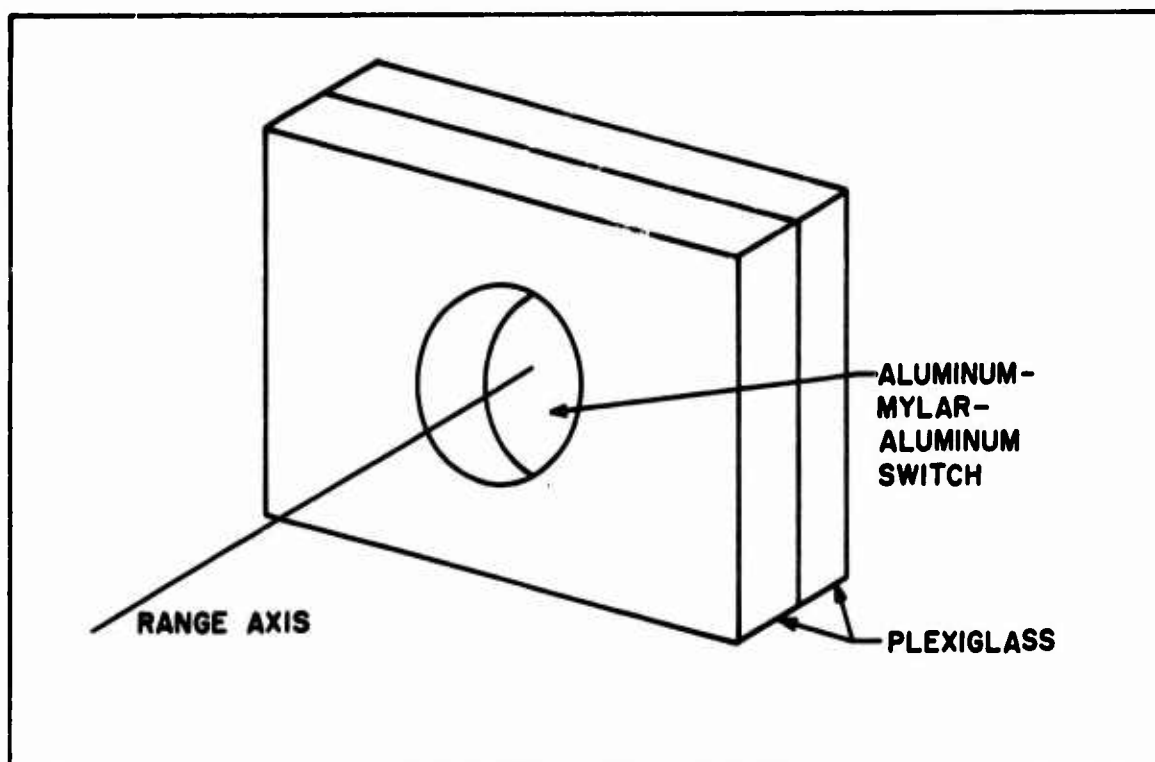


Fig. 41. Foil Contact Switch

one to ground and the other to plus 600 volts. (300 volts was used for the calibration switches.)

The switches used with the flyer plate experiments were made as thin as possible to reduce projectile disruption to an absolute minimum. They consisted of two layers of 6.5 μ thick aluminum separated by a 6.5 μ thick layer of mylar plastic (Fig. 41).

Appendix B

Flyer Plate Test Series

The preliminary experiments for determination of a suitable flyer plate experimental arrangement consisted of five rounds. Each round was designed for the impact of 3.18 mm copper spheres on .79 mm thick copper plates. The results of these tests are presented in order of occurrence.

AFML Round No. 2352

The rigid plate shown in Fig. 42 was used as the support for eleven flyer plates in this test. Unlike the primary tests, four of the flyer plates were half the standard thickness but had standard cross sectional areas. The flyer plates were positioned 10.16 cm from the bumper. The x-ray circuitry was the same as that shown in Fig. 8. The x-ray films were placed below the flyer plates in two 12.7 cm x 17.8 cm rigid cassettes. These two films were to be exposed sequentially at pre-determined times.

A backup plate of 5.08 cm thick styrofoam was used to catch the flyer plates after impact. Some of the plates were imbedded in the styrofoam and others bounced off. Styrofoam was used to avoid flyer plate damage and possible invalidation of the reweighing data. Fig. 43 demonstrates the effect of the debris cloud upon the backup

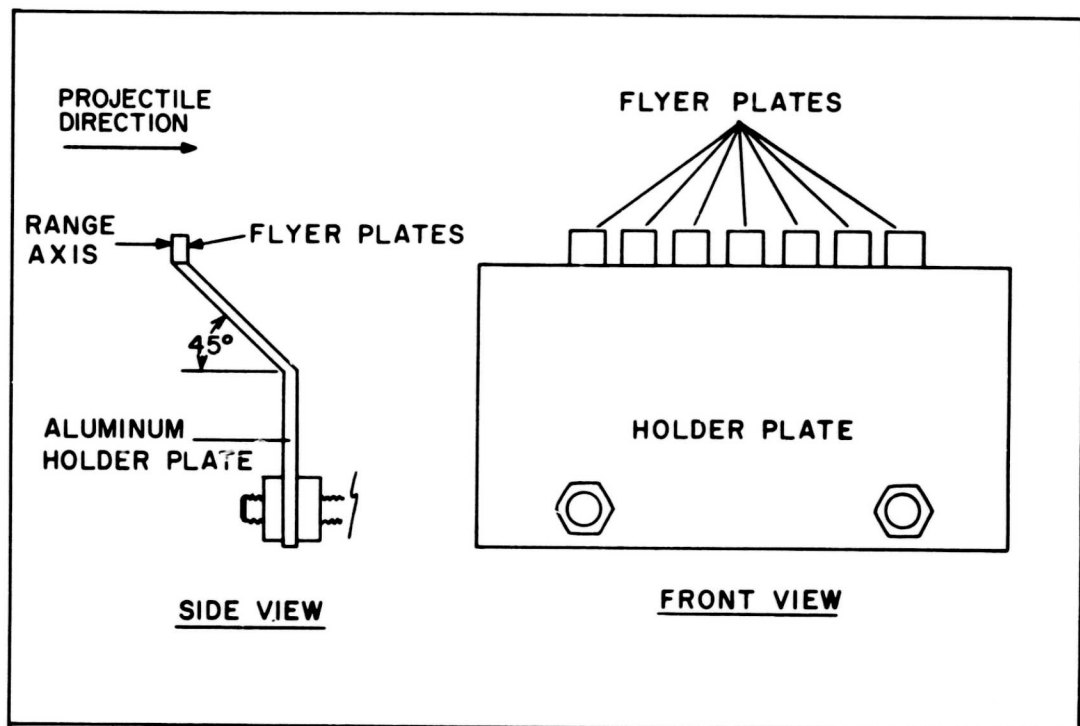


Fig. 42. Rigid Flyer-Plate Holder

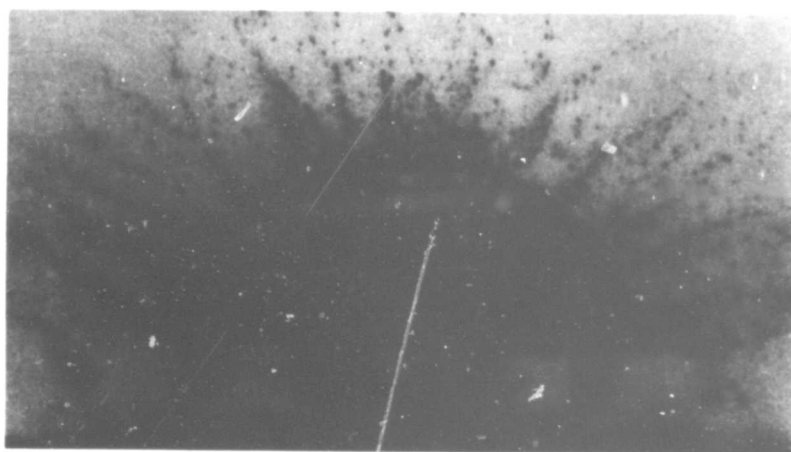


Fig. 43. Impact Effect on Backup Plate

plate. The interesting point is the shadows of the plates on the backup plate indicating that the flyer plates are catching the debris as intended. Flyer plates very often impacted within their own shadow.

No results were obtained from the x-ray system. It was later discovered that the time delays were reversed. The impacts of the flyer plates on the backup plate of styrofoam were located in an arc with the center plate impacting approximately 10 cm high. This led to the rejection of the rigid plate as a means for holding the flyer plates during impact. The rigid plate apparently imparted a vertical velocity to the flyer plates. Weight change data for Round No. 2352 are recorded in Table VI.

AFML Round No. 2357

A new holder system was designed for use in this test. A thin strip of aluminum foil was mounted between two sets of plexiglass clamps. This method (see Fig. 5) was used in the primary experiments. Two x-ray films (44 cm x 11.4 cm) were located lengthwise in place of the other cassettes.

Seven standard size flyer plates were mounted 5.08 cm from the bumper for this test. The time delays were adjusted to account for the increased momentum for each plate caused by their closer proximity to the bumper impact point. The single x-ray obtained was helpful in future experiments and preliminary calculations were

proven approximately correct. The spacing (5.08 cm) and the use of two separate films proved unsatisfactory. The center plate was torn into two pieces with a loss of over 40 percent of its original mass. Table VII contains data from this test. The two velocities shown in Table VII for plate No. 4 are the velocities of the two pieces created by the intense center impact.

AFML Round No. 2365

A ten-flyer plate configuration was used in this test in an attempt to get two x-rays of the plates on one film. One of the small cassettes used in Round 2352 was used. Only one x-ray fired in this round also. Data from this round are shown in Table VIII.

AFML Round No. 2375

A new x-ray film cassette (19 cm x 38 cm) was substituted for this test round. Fourteen flyer plates in the configuration (see Fig. 6) used for the primary rounds were used for the first time. One x-ray fired yielding the results shown in Table IX.

AFML Round No. 2380

In an attempt to obtain good sequential information of the flyers in flight, a high speed framing camera was added to the experimental setup. Good results were obtained with the x-rays and camera. The camera film was not analyzed. Data from the x-rays are presented in Table

X. Eight flyer plates were used for this experiment, because there were not enough plates available for a fourteen plate configuration. The actual camera setup consisted of a mirror through which the camera monitored the flyer plates. The light from a light source located next to the camera was reflected by reflecting paper mounted below the plane of flyer plate trajectories. The reflected light illuminated the flyer plates and yielded a good picture of the plates.

The framing camera proved to be highly satisfactory for the plate measurements. The camera is a source of several sequential pictures which can be used for a more accurate velocity measurement. The camera used in this test burned a bearing and thus was eliminated from further use.

The final experimental configuration determined by these preliminary experiments consisted of the two sequential x-rays, the foil plate holder, and fourteen flyer plates. The flyer plates used in the test series are shown after impact in Fig. 44. The damage distribution can be seen in this figure.

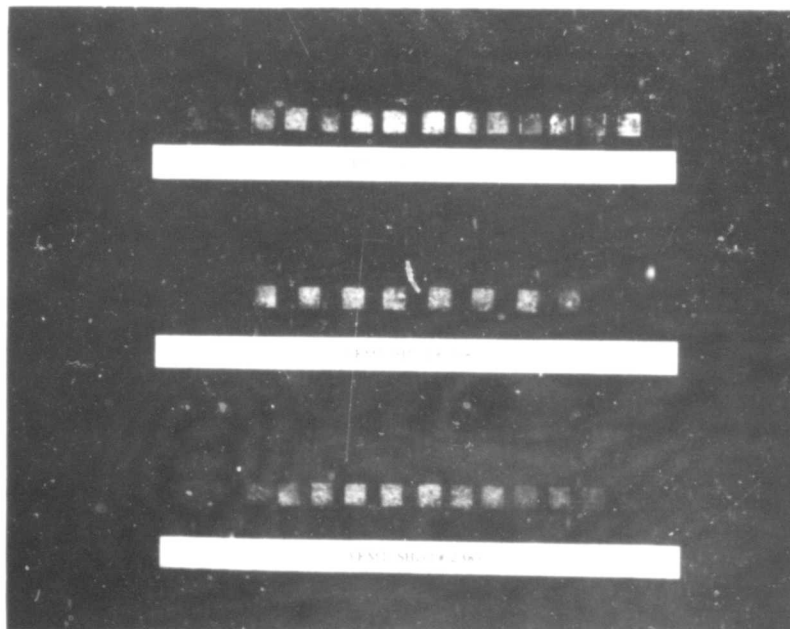
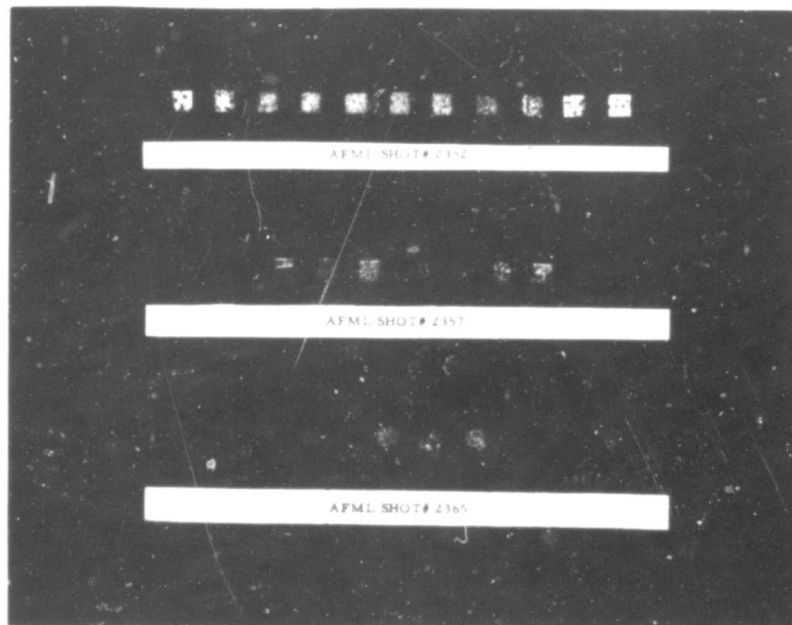


Fig. 44. Photographs of Impacted Flyer Plates

Plate Number	1	2	3	4	5	6	7	8	9	10	11
Initial Mass (mg)	327.1	322.5	323.7	324.8	321.2	326.7	328.9	161	165.9	158	161
Final Mass (mg)	326.2	319.3	318.4	312.9	311.6	321.6	326.3	160.4	165.5	157.2	160.8

Weight Loss Data AFML Round #2352
Table VI

Plate Number	Distance to Cloud Center (cm)	Initial Mass (mg)	Final Mass (mg)	Velocity m/sec	Momentum gm cm/sec	Momentum Intensity (Taps)
1	4.29	327.4	327.4	6	196	486
2	3.12	328.8	323.1	11	355	880
3	1.92	327.3	311.5	36	1120	2777
4	.93	328.0	174.2*	105/99	2800	6944
5	1.13	329.6	318.3	UNOBSERVED		
6	2.22	327.8	325.0	14	455	1128
7	3.43	325.0	324.7	4	130	322

Flyer Data AFML Round #2357

Table VII

Plate Number	Distance to Cloud Center (cm)	Initial Mass (mg)	Final Mass (mg)	Velocity m/sec	Momentum gm cm/sec	Momentum Intensity (Taps)
1	2.7	329.1	327.1	3.17	103.7	257
2	1.33	323.8	316.9	25.4	805	1996
3	.16	329.3	322.9	54	1745	4328
4	1.11	323.9	315.6	32.7	1030	2554
5	2.38	330.6	326.6	11.9	388	962
6	3.65	293.0	291.9	3.18	93	230
7	4.92	167.3	167.2	160	10	248
8	6.69	166.2	166.2	0	0	0
9	3.97	187.8	186.6	5.6	104.5	259
10	4.24	166.1	166.0	.6	9.5	24.7

Flyer Data AFML Round #2365

Table VIII

Plate Number	Distance to Cloud Center (cm)	Initial Mass (mg)	Final Mass (mg)	Velocity (m/sec)	Momentum Intensity (Taps)
1	6.56	344	343.5	3.5	298.2
2	5.60	344.3	343.4	4	341
3	4.64	342.4	340.8	6.8	570
4	3.68	345.1	342.9	9	765
5	2.72	343.4	335.2	19.25	1600
6	1.76	330.6	326.6	26	2106
7	.80	346.2	332.9	46	3756
8	.32	344.4	334.5	63.8	5288
9	1.27	325.8	321.7	40	3191
10	2.23	347.1	343.5	25	2130
11	3.19	345.5	344.5	19.5	1666
12	4.15	349.2	348.5	12.5	1080
13	5.11	348.9	348.2	7.5	647
14	6.07	350.0	349.5	5.5	477

Flyer Data AFML Round #2375

Table IX

Plate Number	Distance to Cloud Center (cm)	Initial Mass (mg)	Final Mass (mg)	Velocity (m/sec)	Momentum Intensity (Taps)
1	4.29	345.5	343.6	13.5	1150
2	3.02	349.3	345.8	18.5	1590
3	1.75	345.3	338.9	30	2520
4	.48	339.7	338.9	76.8	6205
5	.80	346.9	325.9	61.5	5112
6	2.07	336.7	332.9	26.0	2146
7	3.34	343.5	340.2	19	1603
8	4.61	349.8	349.8	8.8	758

Flyer Data AFML Round #2380

Table X

Appendix C

Ballistic Pendulum Calibration

The ballistic pendulum was calibrated with the air rifle setup shown schematically in Fig. 45. A projectile of known mass was fired through three contact switches into the pendulum. The three switches were connected to a pulser unit which registered the contact pulses on an oscilloscope (see Fig. 46). The final velocity of each projectile was computed assuming an equal loss of energy at each switch. The results of the calibration are presented in Table XI. The maximum agreement error was approximately four percent.

Logarithmic Decrement

Damping forces within the suspension system of the ballistic pendulum require adjustment of any measurement made with the pendulum. In free swing, the pendulum loses part of its amplitude on each successive swing. It can thus be classified in the category of a damped free vibration for at least one quarter of its period,

The logarithmic decrement is defined as the log of the ratio of the amplitudes of two successive steps.

$$d = \ln \frac{x_1}{x_2}$$

where d is the logarithmic decrement
 x_1 = amplitude of swing one,
and x_2 = amplitude of swing two.

(Ref 12: 51)

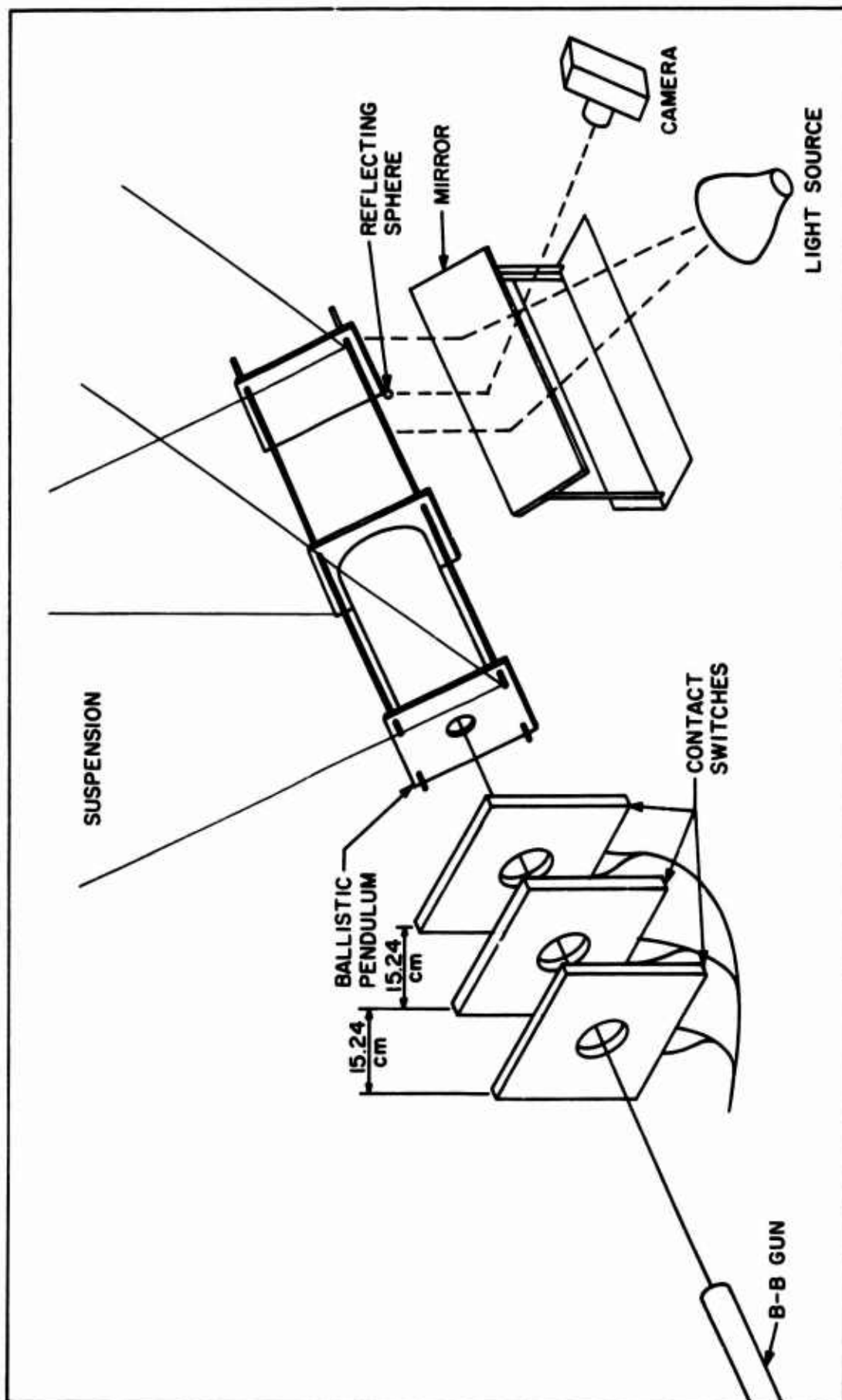


Fig. 45. Pendulum Calibration Configuration

Direct Measurement				Pendulum		Difference in %
Round Number	Projectile Mass (mg)	Velocity m/sec	Momentum gm cm/sec	Mass (gm)	Verticle Motion (cm)	
1	340.7	77.7	2645	244	.055	4%
2	347.3	79.4	2750	244	.0594	4%
3	349.9	79.0	2770	244	.0637	1.8%

Pendulum Calibration Data

Table XI

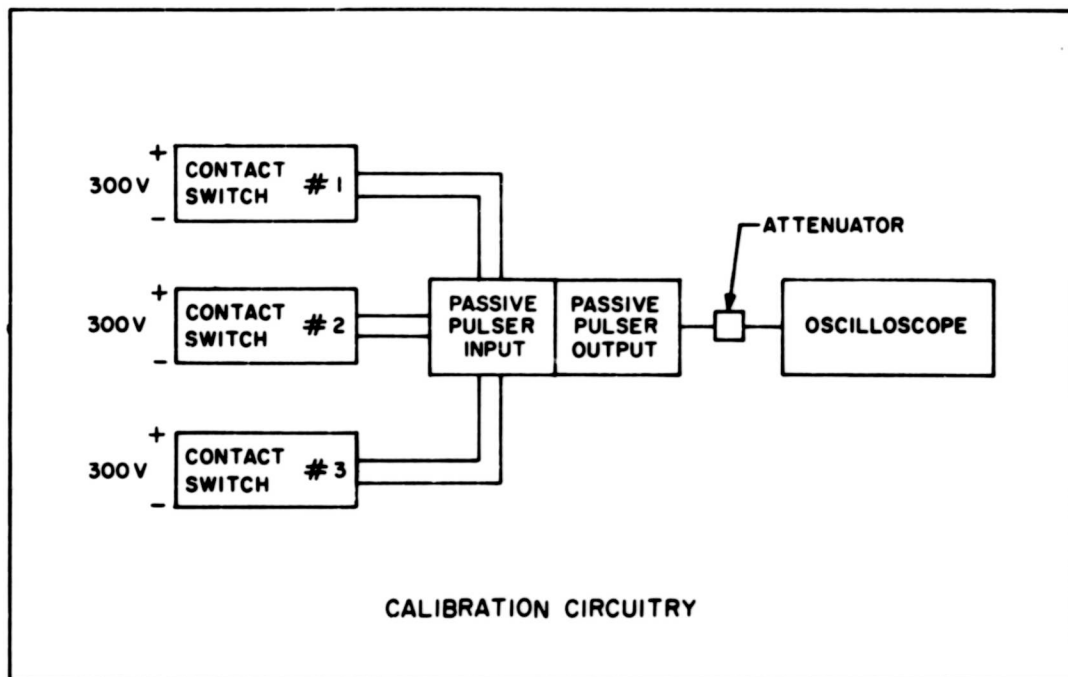


Fig. 46. Calibration Circuit Diagram

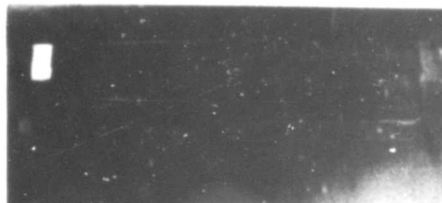
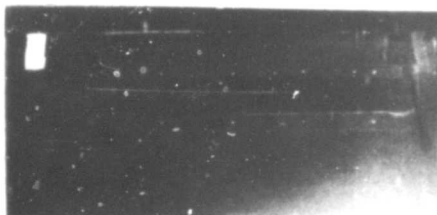
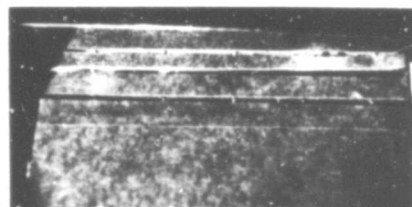


Fig. 47. Photographs for Decrement Calculations

The determination of the decrement was accomplished for each amplitude measured and for each pendulum arrangement. The loss of momentum due to the damping of the pendulum was accounted for by the addition of twenty-five percent of the momentum loss for one cycle. Figure 47 contains photographs of the pendulum movement which were used for the decrement calculations. Close observation can reveal the successive amplitudes of the swing. The decrement measurements were read in the same manner as the momentum measurements. Successive amplitudes were measured and the decrement for each interval was calculated. The correction for one quarter of a cycle was then added to measured values to obtain a corrected value.

Deviation Analysis

After the detection of obvious deviations of the pendulum movement from a straight line motion in the high amplitude swings, a test was conducted to establish a means of determining the effect of the deviations. The calibration range was utilized to fire a projectile into the pendulum center of gravity from an angle of 90° to the pendulum. A sticky clay compound was used to trap the projectile.

The purpose of the test was to attempt to measure the momentum of the projectile by observing the sideward motion of the pendulum. This was completed. The vertical motion of the pendulum center of gravity was calculated using

geometrical relations. The calculated momentum was 2470 gm cm/sec which corresponds favorably with previous calibration measurements.

The sideward motions of the pendulum caused by off center impacts were then analyzed in the same manner. The movement of the center of gravity was again determined from geometrical analysis. The impacts were to the right of the axis of symmetry causing the pendulum to rotate. The point of rotation was assumed to be the center of the rear impacted polyethylene plate. The movement of the rear phenolic plate was then related to the movement of the center of gravity (see Fig. 48).

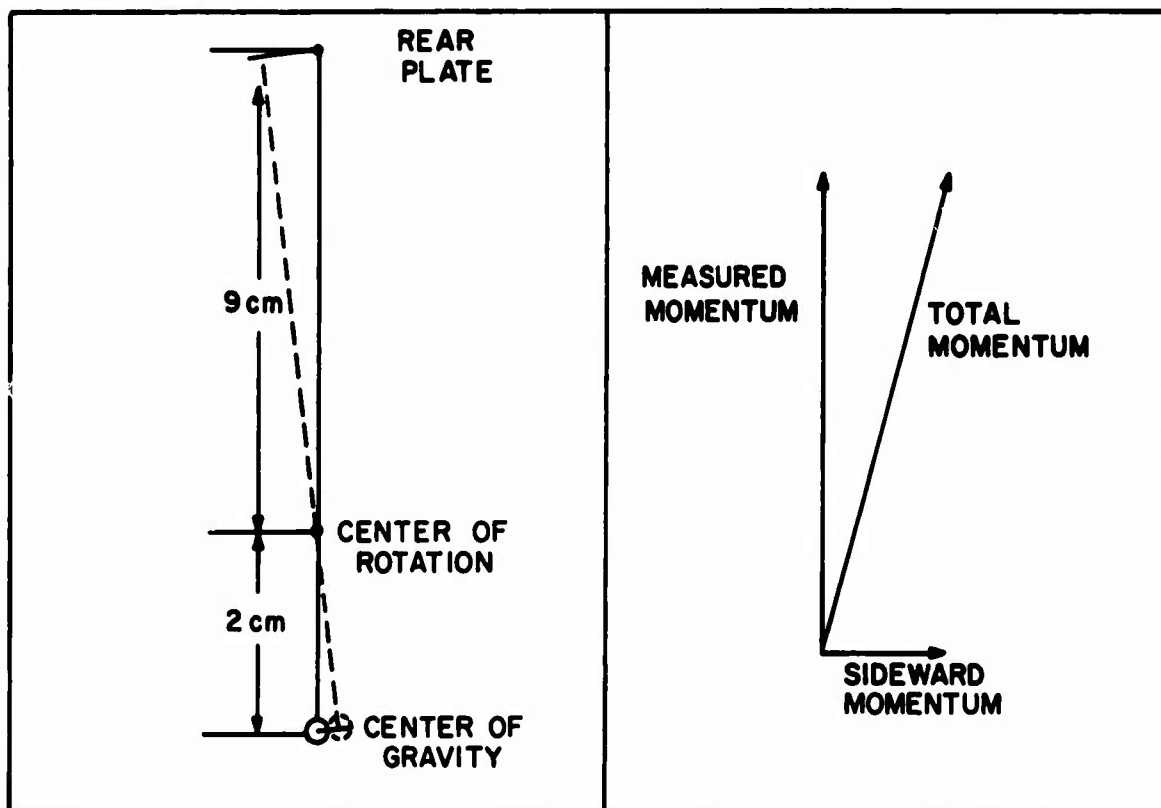


Fig. 48. Geometry of Deviation Analysis

The total momentum was then calculated by using vector addition of the actual measured momentum and the sideward momentum determined from the deviation measurement. The pendulum results were then adjusted.

The actual effect of the sideward motion is demonstrated in Table XII. The required adjustments to the measured momentum were minor except for the adjustment for Round No. 2474.

Round No.	Deviation (cm)	Vertical Motion of Center of Gravity (cm)	Momentum: Measured Sideward Momentum gm cm/sec	Corrected Momentum	
2465	<u>*</u>	<u>*</u>	400 _b	2905	2946
2466	<u>*</u>	<u>*</u>	600 _b	3719	3771
2467	<u>*</u>	<u>*</u>	400 _b	2731	2769
2468	.012	.0005	226	2083	2090
2469	<u>*</u>	<u>*</u>	400 _b	2742	2780
2470	.021	.0008	302	668	698
2471	.047	.0019	458	1685	1720
2472	.012	.0005	229	910	932
2473	.014	.00058	247	981	1000
2474	.024	.0010	322	303	420
2475	.082	.0033	600	3460	3530

* No measurable deviation due to faint traces

b Indicates assumed deviations

Results of Deviation Analysis

Table XII

Appendix D

Table Summary of Flyer Plate and Ballistic Pendulum Rounds

Round Number	Material	Projectile Mass (mg)	Projectile Velocity (km/sec)	Experiment	Results
2352	OFHC Cu	149.40	7.114	Flyer Test	No x-rays
2357	OFHC Cu	147.6	7.144	Flyer Test	1 x-ray
2365	OFHC Cu	147.6	7.133	Flyer Test	1 x-ray
2375	OFHC Cu	148.2	6.899	Flyer Test	1 x-ray
2380	OFHC Cu	148.8	6.953	Flyer Test	2 x-ray, camera
2383	OFHC Cu	148.8	6.652	Primary Round	2 x-ray
2402	2017 Al	46.0	7.254	Primary Round	Good Results
2403	Cd	-----	-----	Primary Round	x-rays exposed
2406	Cd	156.5	7.054	Primary Round	Good Results
2465	OFHC Cu	155.14	6.659	Ballistic Pend	Paint Reading
2466	Cd	156.76	6.757	Ballistic Pend	Good Results
2467	2017 Al	45.82	6.797	Ballistic Pend	Good Results
2468	OFHC Cu	157.93	6.842	Ballistic Pend	Good Results
2469	Cd	153.69	6.655	Ballistic Pend	Good Results

Table XIII

cont'd

Round Number	Material	Projectile Mass (mg)	Projectile Velocity (km/sec)	Experiment	Results
2470	2017 Al	45.80	6.787	Ballistic Pend	Good Results
2471	OFHC Cu	153.17	6.776	Ballistic Pend	Good Results
2472	OFHC Cu	156.89	6.816	Ballistic Pend	Good Results
2473	Cd	153.6	6.720	Ballistic Pend	Good Results
2474	2017 Al	46.08	6.931	Ballistic Pend	Good Results
2475	OFHC Cu	157.93	6.746	Ballistic Pend	Good Results

Table XIII

Summary of Flyer Plate and Ballistic Pendulum Rounds

Unclassified
Security Classification

DOCUMENT CONTROL DATA - R&D		
<small>(Security classification of title, body of abstract and indexing annotation must be entered when the overall report is classified)</small>		
1. ORIGINATING ACTIVITY (Corporate author) Air Force Materials Laboratory Wright-Patterson AFB, Ohio 45433		2a. REPORT SECURITY CLASSIFICATION Unclassified
		2b. GROUP
3. REPORT TITLE MOMENTUM DISTRIBUTION IN THE DEBRIS CLOUD PRODUCED BY HYPERVELOCITY PERFORATION OF THIN PLATES		
4. DESCRIPTIVE NOTES (Type of report and inclusive dates) Technical Report		
5. AUTHOR(S) (Last name, first name, initial) Cunningham, John H., Captain, USAF		
6. REPORT DATE July 1968	7a. TOTAL NO. OF PAGES 86	7b. NO. OF REFS 12
8a. CONTRACT OR GRANT NO.	9a. ORIGINATOR'S REPORT NUMBER(S) AFML-TR-68-174	
b. PROJECT NO. 7360		
c. Task No. 736006	9b. OTHER REPORT NO(S) (Any other numbers that may be assigned this report) AFIT Thesis GSF/MC/68-4	
10. AVAILABILITY/LIMITATION NOTICES This document has been approved for public release and sale; its distribution is unlimited.		
11. SUPPLEMENTARY NOTES	12. SPONSORING MILITARY ACTIVITY Air Force Materials Laboratory Air Force Systems Command Wright-Patterson AFB, Ohio 45433	
13. ABSTRACT An experimental investigation of the momentum distribution within the debris cloud produced by the impact of 3.17 mm spheres on 0.79 mm thick plates was conducted. Two independent experiments with projectile velocities ranging from 6.65 km/sec to 7.25 km/sec were completed in an attempt to determine momentum distribution. Small metal plates were impacted by the cloud for measurement of the incident momentum. A ballistic pendulum was used in an attempt to capture small segments of the debris cloud and to measure the momentum distribution in the cloud itself. The momentum intensity, as a function of distance from the center of the debris cloud, was determined in each experiment and the results were compared and evaluated.		

14 KEY WORDS	LINK A		LINK B		LINK C	
	ROLE	WT	ROLE	WT	ROLE	WT
Hypervelocity Impact Thin Plates Debris Cloud Momentum Distribution						

INSTRUCTIONS

1. **ORIGINATING ACTIVITY:** Enter the name and address of the contractor, subcontractor, grantee, Department of Defense activity or other organization (*corporate author*) issuing the report.

2a. **REPORT SECURITY CLASSIFICATION:** Enter the overall security classification of the report. Indicate whether "Restricted Data" is included. Marking is to be in accordance with appropriate security regulations.

2b. **GROUP:** Automatic downgrading is specified in DoD Directive 5200.10 and Armed Forces Industrial Manual. Enter the group number. Also, when applicable, show that optional markings have been used for Group 3 and Group 4 as authorized.

3. **REPORT TITLE:** Enter the complete report title in all capital letters. Titles in all cases should be unclassified. If a meaningful title cannot be selected without classification, show title classification in all capitals in parenthesis immediately following the title.

4. **DESCRIPTIVE NOTES:** If appropriate, enter the type of report, e.g., interim, progress, summary, annual, or final. Give the inclusive dates when a specific reporting period is covered.

5. **AUTHOR(S):** Enter the name(s) of author(s) as shown on or in the report. Enter last name, first name, middle initial. If military, show rank and branch of service. The name of the principal author is an absolute minimum requirement.

6. **REPORT DATE:** Enter the date of the report as day, month, year; or month, year. If more than one date appears on the report, use date of publication.

7a. **TOTAL NUMBER OF PAGES:** The total page count should follow normal pagination procedures, i.e., enter the number of pages containing information.

7b. **NUMBER OF REFERENCES:** Enter the total number of references cited in the report.

8a. **CONTRACT OR GRANT NUMBER:** If appropriate, enter the applicable number of the contract or grant under which the report was written.

8b, 8c, & 8d. **PROJECT NUMBER:** Enter the appropriate military department identification, such as project number, subproject number, system numbers, task number, etc.

9a. **ORIGINATOR'S REPORT NUMBER(S):** Enter the official report number by which the document will be identified and controlled by the originating activity. This number must be unique to this report.

9b. **OTHER REPORT NUMBER(S):** If the report has been assigned any other report numbers (*either by the originator or by the sponsor*), also enter this number(s).

10. **AVAILABILITY/LIMITATION NOTICES:** Enter any limitations on further dissemination of the report, other than those

imposed by security classification, using standard statements such as:

- (1) "Qualified requesters may obtain copies of this report from DDC."
- (2) "Foreign announcement and dissemination of this report by DDC is not authorized."
- (3) "U. S. Government agencies may obtain copies of this report directly from DDC. Other qualified DDC users shall request through _____."
- (4) "U. S. military agencies may obtain copies of this report directly from DDC. Other qualified users shall request through _____."
- (5) "All distribution of this report is controlled. Qualified DDC users shall request through _____."

If the report has been furnished to the Office of Technical Services, Department of Commerce, for sale to the public, indicate this fact and enter the price, if known.

11. **SUPPLEMENTARY NOTES:** Use for additional explanatory notes.

12. **SPONSORING MILITARY ACTIVITY:** Enter the name of the departmental project office or laboratory sponsoring (*paying for*) the research and development. Include address.

13. **ABSTRACT:** Enter an abstract giving a brief and factual summary of the document indicative of the report, even though it may also appear elsewhere in the body of the technical report. If additional space is required, a continuation sheet shall be attached.

It is highly desirable that the abstract of classified reports be unclassified. Each paragraph of the abstract shall end with an indication of the military security classification of the information in the paragraph, represented as (TS), (S), (C), or (U).

There is no limitation on the length of the abstract. However, the suggested length is from 150 to 225 words.

14. **KEY WORDS:** Key words are technically meaningful terms or short phrases that characterize a report and may be used as index entries for cataloging the report. Key words must be selected so that no security classification is required. Identifiers, such as equipment model designation, trade name, military project code name, geographic location, may be used as key words but will be followed by an indication of technical context. The assignment of links, rules, and weights is optional.